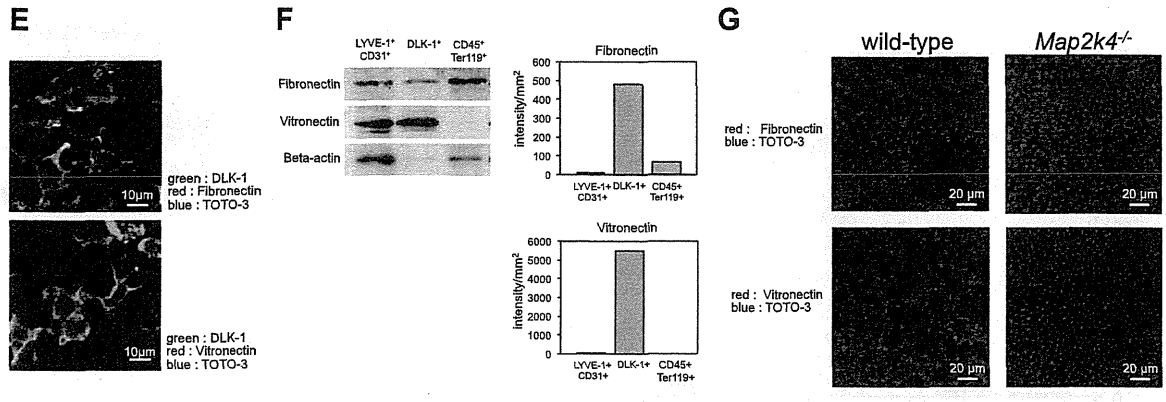

Fig. 3 – continued

which fetal liver component contributes to ECM-production, expression of genes encoding ECM factors was examined in hepatoblasts, sinusoid endothelial cells and hematopoietic cells by real-time PCR. All ECM genes analyzed, including *laminin B 1 (Lamb1)*, *laminin, beta2 (Lamb2)*, *Vtn*, *Fn1* and *tenascin C (Tnc)*, were highly expressed in hepatoblasts compared to sinusoid endothelial cells and hematopoietic cells (Fig. 3D). Both Fibronectin and Vitronectin were detected in fetal liver at 12.5 dpc by immunohistochemistry (Fig. 3E). In addition, Western blot analysis showed that hepatoblasts expressed Vitronectin and Fibronectin proteins at levels higher than those seen in sinusoid endothelial cells and hematopoietic cells (Fig. 3F). To characterize hepatoblast function in fetal liver, we analyzed *Map2k4 (mitogen-activated protein kinase kinase* 4, formerly known as *Sek1* and *MKK4*)$^{-/-}$ mouse embryos, which lack fetal liver hepatoblasts (Nishina et al., 1997a, 1997b, 1999; Watanabe et al., 2002). Immunohistochemistry indicated that expression of Fibronectin and Vitronectin proteins was lower relative to that seen in wild-type mouse embryos in fetal liver of *Map2k4*$^{-/-}$ mouse embryos (Fig. 3G). Both mRNA and protein expression data and analysis of mutant embryos suggest that hepatoblasts expressing DLK-1 are primarily responsible for ECM production in fetal liver.

3.3. *Regulation of ECM production by TGF-beta-1*

We next asked how ECM production in hepatoblasts is regulated. Based on findings suggesting that TGF-betas and HGF regulate ECM production (Nakamura et al., 1992; Ziyadeh et al., 1994; Chimal-Monroy and Diaz de Leon, 1999; Laping et al., 2002; Gaggioli et al., 2005), we analyzed gene expression of *Tgfb1*, *Tgfb2*, *Tgfb3* and *Hgf* in whole fetal liver samples at 12.5 and 14.5 dpc (Fig. 4A). *Tgfb1* was predominantly expressed in fetal liver at both stages. TGF-beta-1 protein was also detected by Western blot analysis in fetal liver at 12.5 dpc (Fig. 4B). To investigate whether TGF-beta-1 and HGF signals regulate ECM production in fetal liver, we used real-time PCR to examine expression of *Tgfb1* and *Tgfbr2*, which encodes the TGF-beta receptor type 2 (TGFR-2), and *Hgf* and *Met*, which encodes HGF receptor, in hepatoblasts, sinusoid endothelial cells and hematopoietic cells. *Tgfb1* was predominantly expressed in sinusoid endothelial cells and hematopoietic cells, whereas *Tgfbr2* was predominantly expressed in both sinusoid endothelial cells and hepatoblasts (Fig. 4C). Western blot analysis showed that TGF-beta-1 protein was highly expressed in both hepatoblasts and sinusoid endothelial cells (Fig. 4D). *Tgfb1* and *Tgfbr2* expression was detected in HSCs and at each stage of differentiated erythroid cells isolated from fetal liver at 12.5 dpc (Fig. S2). By contrast, both *Hgf* and *Met* were predominantly expressed in hepatoblasts. Flow cytometric analysis also showed that TGFR-2 and HGF receptor proteins were expressed in 56.2% and 68.5% of hepatoblasts, respectively (Fig. 3C).

To further investigate which signal functions in ECM production, TGFR2 inhibitors were administered to mouse embryos using an intra-cardiac injection technique that we developed for use in 10.0–10.5 dpc embryos (Sugiyama et al., 2003, 2005; Sasaki et al., 2010). After hepatoblasts develop in fetal liver, circulating hematopoietic cells home to fetal liver after 9.5 dpc (Johnson and Jones, 1973; Johnson and Moore, 1975; Houssaint, 1981; Cudennec et al., 1981; Sugiyama et al., 2005). To rule out effects of ECM gene expression by hematopoetic cells (Fig. 3D), we chose to inject inhibitors at 10.25 dpc, when fetal liver is predominantly comprised of hepatoblasts. Following injection, we maintained embryos for variable time periods in a whole embryo culture system (Osumi-Yamashita et al., 1997; Kulkeaw et al., 2009). Twelve hours after injection of a specific, cell-permeable TGF-beta receptor type-1 Kinase Inhibitor, *Vtn*, *Fn1* and *Tnc* expression levels were down-regulated relative to controls (Fig. 5A). Injection of a different TGF-beta receptor type-1 Kinase Inhibitor II promoted a detectable decrease in *Vtn* expression by 6 h of culture and significant decreases in *Vtn*, *Fn1* and *Tnc* expression levels relative to controls after 12 h of culture (Fig. 5B). TGF-beta receptor type-1, also known as ALK5, binds to both growth differentiation factor-1 (GDF1) and TGF-betas. To determine whether down-regulation of ECM genes resulted from specific alterations in TGF-beta-1 signaling, anti-TGF-beta-1 blocking antibody was injected into mouse embryos. As shown in Fig. 5C, *Vtn*, *Fn1* and *Tnc* expression was down-regulated after 12 h of whole embryo culture. To confirm that TGF-beta-1 signaling is down-regulated after administration of anti-TGF-beta-1 blocking antibody, injected embryos were stained with anti-phosphorylated SMAD3 antibody. A 19.4% decrease in SMAD-phosphorylation was observed after injection of

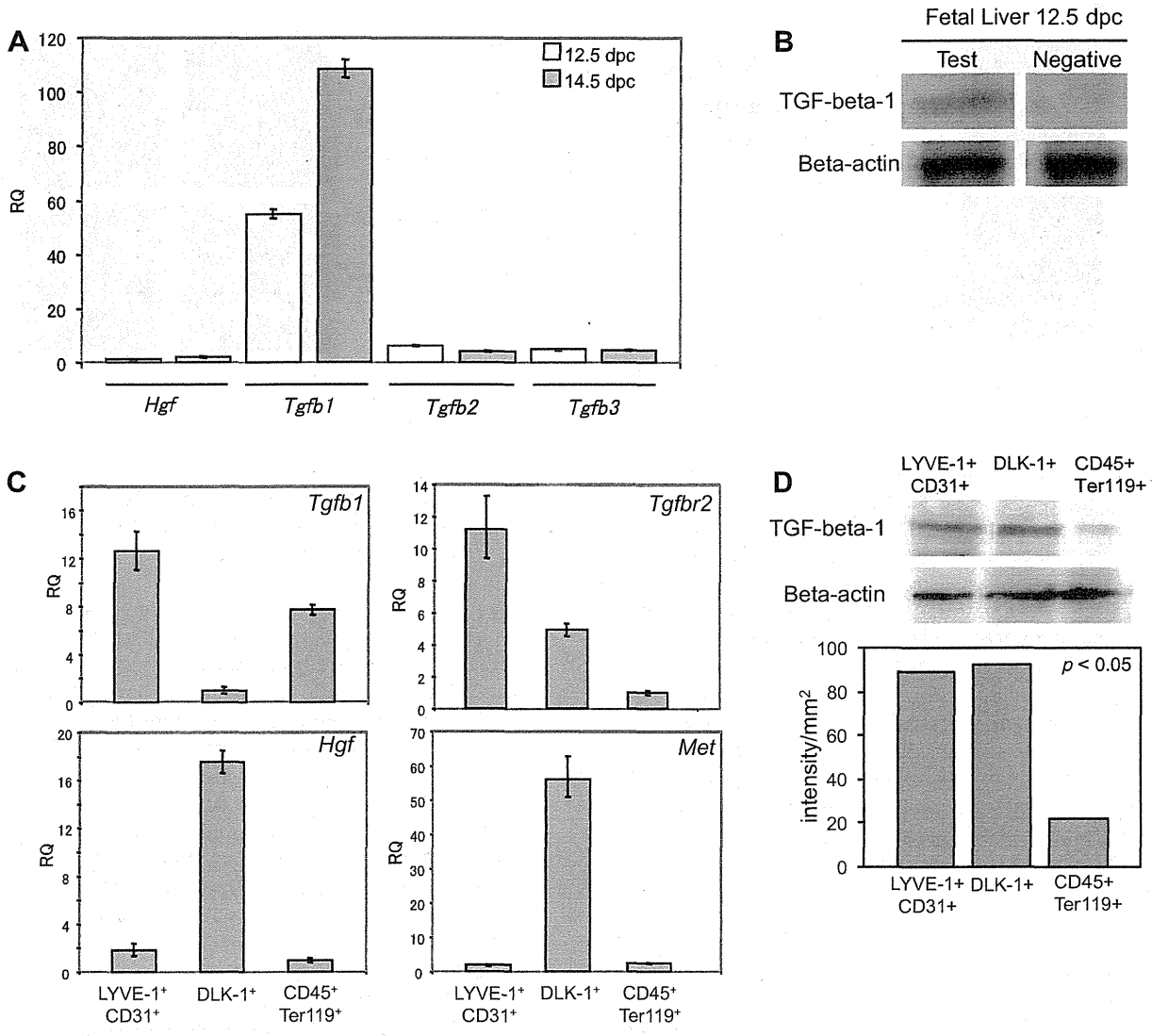

Fig. 4 – TGF-beta and HGF expression in fetal liver. (A) Expression of *Tgfb1*, *Tgfb2*, *Tgfb3* and *Hgf* was examined in fetal liver samples at 12.5 and 14.5 dpc. *Tgfb1* was highly expressed at both stages. (B) TGF-beta-1 protein was detected by Western blot analysis of fetal liver at 12.5 dpc. (C) Expression of *Tgfb1* and *Tgfbr2*, which encodes its receptor, and *Hgf* and *Met*, which encodes its receptor, was examined by real-time PCR in hepatoblasts, sinusoid endothelial cells and hematopoietic cells according to gates defined in Fig. 3C. *Tgfb1* was predominantly expressed in sinusoid endothelial cells and hematopoietic cells, whereas *Tgfbr2* was highly expressed both in sinusoid endothelial cells and hepatoblasts. Both *Hgf* and *Met* were highly expressed in hepatoblasts. (D) TGF-beta-1 expression was examined by Western blot analysis in each fraction of cells sorted from ICR mouse fetal liver at 12.5 dpc according to gate settings defined in Fig. 3C. Protein expression levels were normalized to Beta-actin and displayed as intensity per mm^2.

anti-TGF-beta-1 blocking antibody (Fig. S3). As shown in Fig. S4, some DLK-1 positive and negative cells were stained with anti-phosphorylated SMAD3 Ab in fetal liver at 10.5 dpc. Taken together, it is likely that TGF-beta-1 signaling in both hepatoblasts expressing DLK-1 and non-hepatoblasts was down-regulated after administration of anti-TGF-beta-1 blocking antibody.

To further investigate how TGF-beta-1 controls ECM production in hepatoblasts, we sorted hepatoblasts expressing DLK-1 and cultured them in the presence of TGF-beta-1. After 6 h of culture, *Vtn*, *Fn1* and *Tnc* expression was up-regulated (Fig. 5D). Taken together, these data strongly suggest that TGF-beta-1/TGFR-2 signaling promotes ECM production by hepatoblasts in fetal liver.

4. Discussion

Hepatoblasts were originally regarded as common progenitors of hepatocytes and biliary epithelial cells and thought to support liver construction through formation of a mesh-like structure (Tanimizu et al., 2003; Sasaki and Sonoda, 2000). Recently, it was reported that expression of SCF and EPO by

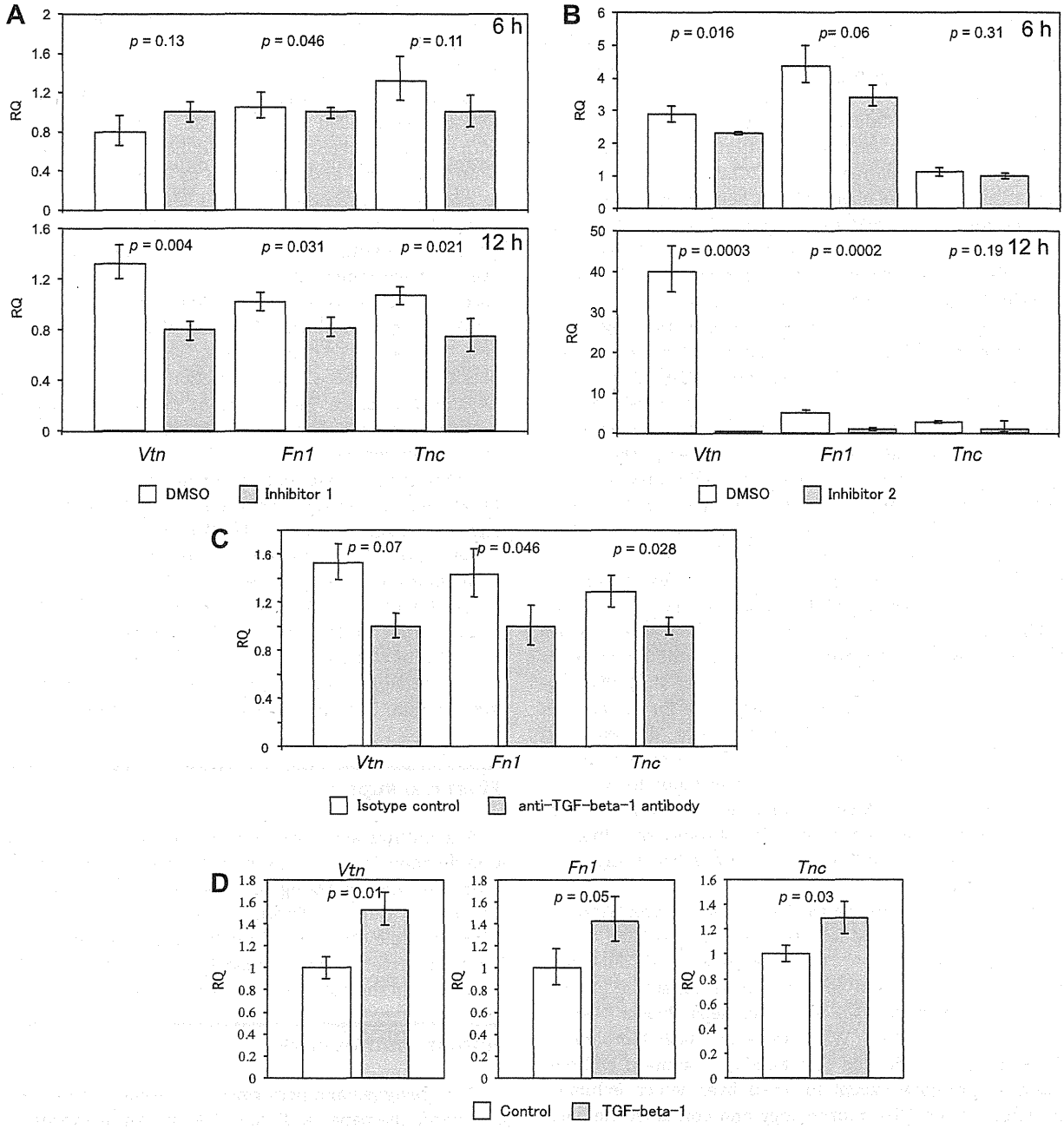

Fig. 5 – Functional analysis of the effect of TGF-beta-1/TGFR2 signaling on ECM production in fetal liver. (A) A TGF-beta receptor type-1 Kinase Inhibitor (inhibitor 1) was administered to ICR mouse embryos at 10.25 dpc by intra-cardiac injection, and embryos were then cultured in a whole embryo culture system. Left and right bars show control (DMSO injection) and sample (inhibitor injection) responses, respectively. Expression of *Vtn*, *Fn1* and *Tnc* genes was slightly down-regulated after 6 h and then more significantly so at 12 h of whole embryo culture compared to controls. (B) TGF-beta receptor type-1 Kinase Inhibitor II (inhibitor 2) was administered as in (A). Expression of *Vtn*, *Fn1* and *Tnc* was slightly and then significantly down-regulated relative to controls after 6 and 12 h of whole embryo culture, respectively. (C) Anti-TGF-beta-1 blocking antibody was administered as in (A). Left and right bars show control (Isotype IgG injection) and sample (blocking antibody injection), respectively. Expression of *Vtn*, *Fn1* and *Tnc* was down-regulated after 12 h of whole embryo culture. (D) Hepatoblasts expressing DLK-1 were sorted from 12.5 dpc fetal liver by flow cytometry and 10,000 cells were cultured with or without TGF-beta-1 (10 ng/mL). *Vtn*, *Fn1* and *Tnc* expression was up-regulated after 6 h of *in vitro* culture with TGF-beta-1.

hepatoblasts promotes HSC expansion and differentiation (Lodish et al., 2010; Sugiyama et al., 2011). ECMs act together with cytokines to maximize cytokine signaling in specific tissues (Hynes and Yamada, 1982; Humphries et al., 1989; Frisch and Ruoslahti, 1997; Taipale and Keski-Oja, 1997).

Based on integrin expression patterns, we hypothesized that their binding partners were ECM proteins. Following comparison of *integrin-alpha* in each hematopoietic cell fraction, we found that *Itga4* and *Itga6* are highly expressed in HSC and BFU-E fractions. It is reported that Integrin alpha-4 accelerates erythroid cell differentiation but does not affect HSC colonization in fetal liver (Yanai et al., 1994; Arroyo et al., 1999). Our data suggest that regulation of erythroid cell differentiation through Integrin alpha-4 occurs primarily at the level of HSCs and BFU-E in fetal liver. We found that *Itga5*, *Itga9* and *ItgaV* were moderately expressed in HSC and BFU-E fractions. Since hematopoietic cells derived from *Itga5*, *Itga9* or *ItgaV* single knockout mice can colonize fetal liver, it is likely that only Integrin beta-1 is specifically required for hematopoietic cell colonization of fetal liver and that various Integrin alpha can substitute for each other to some extent (Taverna et al., 1998; Bader et al., 1998; Huang et al., 2000). In fetal liver, *Vtn* was highly expressed among several ECM genes at both 12.5 and 14.5 dpc, and Vitronectin protein was detected at high levels in hepatoblasts at 12.5 dpc. *Vtn*-deficient mouse embryos reportedly show no abnormalities (Zheng et al., 1995), suggesting that other ECM factors compensate for its loss. On the other hand, *fibronectin*-deficient mice die early in embryogenesis probably due to abnormal mesoderm development (George et al., 1993). Fibronectin binds to Integrins alpha-4/beta-1, alpha-5/beta-1 and alpha-V/beta-1. These results and our gene expression data suggest that Integrin alpha-4/beta-1 and Fibronectin signaling is likely important for HSC differentiation.

Among cells comprising the fetal liver, hepatoblasts predominantly produce ECM factors. Here, we evaluated mouse embryos lacking *Map2k4*$^{-/-}$, the gene encoding the dual specificity mitogen-activated protein kinase kinase 4 protein. These mice reportedly lack fetal liver hepatoblasts (Nishina et al., 1997a, 1997b, 1999; Watanabe et al., 2002). Morphological examination indicated that *Map2k4*$^{-/-}$ mutant embryos developed normally except for their liver, which exhibited an unusual pouch-like morphology and contained hematopoietic cells. The hematopoietic activity of these cells is reportedly normal (Nishina et al., 1999). Although it is formally possible that MAPK signaling could directly impact ECM factor expression, our findings overall strongly suggest that down-regulation of Fibronectin and Vitronectin production is due to loss of hepatoblasts.

We also show that TGF-beta-1/TGFR-2 signaling functions in ECM production by fetal liver cells, predominantly hepatoblasts. TGF-beta-1/TGFR-2 signaling regulates diverse processes such as cell growth, differentiation, and apoptosis in adult animals and in embryogenesis (Shi and Massague, 2003; Watabe et al., 2003; Moustakas and Heldin, 2009). We found that sinusoid endothelial cells, hematopoietic cells and hepatoblasts express TGF-beta-1 mRNA and protein. Flow cytometry analysis showed that TGFR-2 was expressed in 1.8% of hematopoietic cells, 56.2% of hepatoblasts and 99% of sinusoid endothelial cells, suggesting that hepatoblasts and sinusoid endothelial cells are affected by TGF-beta-1/TGFR-2 signaling to a greater extent than hematopoietic cells. The observation that a high proportion of sinusoid endothelial cells expresses TGFR-2 is compatible with previous reports that TGF-beta-1/TGFR-2 signaling controls sinusoid endothelial cell differentiation in addition to normal angiogenesis (Shi and Massague, 2003; Watabe et al., 2003; Moustakas and Heldin, 2009; Yoshida et al., 2007). Interestingly, half of all hepatoblasts expressed TGFR-2, suggesting a functional separation of hepatoblasts based on TGFR-2 expression. Although expression levels of *Tgfb2 and Tgfb3* are lower than that of *Tgfb1* in fetal liver at both 12.5 and 14.5 dpc (Fig. 4A), we cannot exclude the possibility that these factors function in ECM production by hepatoblasts, since *Tgfb1*-deficient mouse embryos exhibit no gross embryonic abnormalities, suggesting a compensatory mechanism (Shull et al., 1992).

Taken together with data showing that TGF-beta-1 up-regulates *Vtn*, *Fn1* and *Tnc* expression *in vitro*, TGF-beta-1/TGFR-2 signaling likely regulates ECM-production in fetal liver hepatoblasts *in vivo*, facilitating interactions with Integrins. In embryos injected with either TGF-beta receptor type-1 Kinase Inhibitor or TGF-beta receptor type-1 Kinase Inhibitor II, the number of fetal liver cells was significantly decreased after 12 h of whole embryo culture (Fig. S5). It is also possible that treatment with TGF-beta-1 inhibitors may alter cell proliferation. That possibility will be investigated in future studies.

Financial support

The authors acknowledge grant support from the Special Coordination Funds for Promoting Science and Technology, a Grant-in-Aid for Young Scientists (B) from The Ministry of Education, Culture, Sports, Science and Technology, a Grant-in-Aid by Ministry of Health, Labor and Welfare, Bilateral Joint Projects for the Japan Society for the Promotion of Science, and the Tokyo Biochemical Research Foundation.

Author contributions

D. S. designed and performed the research, analyzed data and wrote the paper. K. K. and C. M. performed research.

Acknowledgements

We thank the Research Support Center, the Graduate School of Medical Sciences, Kyushu University and Olympus Corporation, for technical support, Drs. T. Suda, K. Akashi and K. Tani for helpful discussion, Dr. T. Inoue, Miss Y. Horio and Miss Tan for technical support, and Dr. Elise Lamar for critical reading of the manuscript.

Appendix A. Supplementary data

Supplementary data associated with this article can be found, in the online version, at http://dx.doi.org/10.1016/j.mod.2012.09.003.

REFERENCES

Arroyo, A.G., Yang, J.T., Rayburn, H., Hynes, R.O., 1999. Alpha4 integrins regulate the proliferation/differentiation balance of multilineage hematopoietic progenitors in vivo. Immunity 11, 555–566.

Bader, B.L., Rayburn, H., Crowley, D., Hynes, R.O., 1998. Extensive vasculogenesis, angiogenesis, and organogenesis precede lethality in mice lacking all alpha v integrins. Cell 95, 507–519.

Chimal-Monroy, J., Diaz de Leon, L., 1999. Expression of N-cadherin, N-CAM, fibronectin and tenascin is stimulated by TGF-beta1, beta2, beta3 and beta5 during the formation of precartilage condensations. Int. J. Dev. Biol. 43, 59–67.

Cudennec, C.A., Thiery, J.P., Le Douarin, N.M., 1981. *In vitro* induction of adult erythropoiesis in early mouse yolk sac. Proc. Natl. Acad. Sci. USA 78, 2412–2416.

Dzierzak, E., Medvinsky, A., de Bruijn, M., 1998. Qualitative and quantitative aspects of hematopoietic cell development in the mammalian embryo. Immunol. Today 19, 228–236.

Ema, H., Nakauchi, H., 2000. Expansion of hematopoietic stem cells in the developing liver of a mouse embryo. Blood 95, 2284–2288.

Frisch, S.M., Ruoslahti, E., 1997. Integrins and anoikis. Curr. Opin. Cell Biol. 9, 701–706.

Gaggioli, C., Deckert, M., Robert, G., Abbe, P., Batoz, M., Ehrengruber, M.U., Ortonne, J.P., Ballotti, R., Tartare-Deckert, S., 2005. HGF induces fibronectin matrix synthesis in melanoma cells through MAP kinase-dependent signaling pathway and induction of Egr-1. Oncogene 24, 1423–1433.

George, E.L., Georges-Labouesse, E.N., Patel-King, R.S., Rayburn, H., Hynes, R.O., 1993. Defects in mesoderm, neural tube and vascular development in mouse embryos lacking fibronectin. Development 119, 1079–1091.

Hirsch, E., Iglesias, A., Potocnik, A.J., Hartmann, U., Fassler, R., 1996. Impaired migration but not differentiation of haematopoietic stem cells in the absence of beta-1 integrins. Nature 380, 171–175.

Houssaint, E., 1981. Differentiation of the mouse hepatic primordium. II. Extrinsic origin of the haemopoietic cell line. Cell Differ. 10, 243–252.

Huang, X.Z., Wu, J.F., Ferrando, R., Lee, J.H., Wang, Y.L., Farese Jr., R.V., Sheppard, D., 2000. Fatal bilateral chylothorax in mice lacking the integrin alpha9beta1. Mol. Cell. Biol. 20, 5208–5215.

Humphries, M.J., Obara, M., Olden, K., Yamada, K.M., 1989. Role of fibronectin in adhesion, migration, and metastasis. Cancer Invest. 7, 373–393.

Hynes, R.O., Yamada, K.M., 1982. Fibronectins: multifunctional modular glycoproteins. J. Cell Biol. 95, 369–377.

Inoue, T., Sugiyama, D., Kurita, R., Oikawa, T., Kulkeaw, K., Kawano, H., Miura, Y., Okada, M., Suehiro, Y., Takahashi, A., Marumoto, T., Inoue, H., Komatsu, N., Tani, K., 2011. APOA-1 is a novel marker of erythroid cell maturation from hematopoietic stem cells in mice and humans. Stem Cell Rev. 7, 43–52.

Johnson, G.R., Jones, R.O., 1973. Differentiation of the mammalian hepatic primordium in vitro. I. Morphogenesis and the onset of haematopoiesis. J. Embryol. Exp. Morphol. 30, 83–96.

Johnson, G.R., Moore, M.A., 1975. Role of stem cell migration in the initiation of mouse foetal liver haemopoiesis. Nature 258, 726–728.

Klein, G., Beck, S., Müller, C.A., 1993. Tenascin is a cytoadhesive extracellular matrix component of the human hematopoietic microenvironment. J. Cell Biol. 123, 1027–1035.

Kulkeaw, K., Mizuochi, C., Horio, Y., Osumi, N., Tsuji, K., Sugiyama, D., 2009. Application of whole embryo culture system on stem cell research. Stem Cell Rev. 5, 175–180.

Laping, N.J., Grygielko, E., Mathur, A., Butter, S., Bomberger, J., Tweed, C., Martin, W., Fornwald, J., Lehr, R., Harling, J., Gaster, L., Callahan, J.F., Olson, B.A., 2002. Inhibition of transforming growth factor (TGF)-beta1-induced extracellular matrix with a novel inhibitor of the TGF-beta type I receptor kinase activity: SB-431542. Mol. Pharmacol. 62, 58–64.

Lodish, H., Flygare, J., Chou, S., 2010. From stem regulation of red cell production at multiple levels by multiple hormones. Life 62, 492–496.

Long, M.W., Dixit, V.M., 1990. Thrombospondin functions as a cytoadhesion molecule for human hematopoietic progenitor cells. Blood 75, 2311–2318.

Long, M.W., Briddell, R., Walter, A.W., Bruno, E., Hoffman, R., 1992. Human hematopoietic stem cell adherence to cytokines and matrix molecules. J. Clin. Invest. 90, 251–255.

Moustakas, A., Heldin, C.H., 2009. The regulation of TGF-b signal transduction. Development 136, 3699–3714.

Mouta Carreira, C., Nasser, S.M., di Tomaso, E., Padera, T.P., Boucher, Y., Tomarev, S.I., Jain, R.K., 2001. LYVE-1 is not restricted to the lymph vessels: expression in normal liver blood sinusoids and down-regulation in human liver cancer and cirrhosis. Cancer Res. 61, 8079–8084.

Nakamura, T., Miller, D., Ruoslahti, E., Border, W.A., 1992. Production of extracellular matrix by glomerular epithelial cells is regulated by transforming growth factor-beta 1. Kidney Int. 41, 1213–1221.

Nishina, H., Bachmann, M., Oliveira-dos-Santos, A.J., Kozieradzki, I., Fischer, K.D., Odermatt, B., Wakeham, A., Shahinian, A., Takimoto, H., Bernstein, A., Mak, T.W., Woodgett, J.R., Ohashi, P.S., Penninger, J.M., 1997a. Impaired CD28-mediated interleukin 2 production and proliferation in stress kinase SAPK/ERK1 kinase (SEK1)/mitogen-activated protein kinase kinase 4 (MKK4)-deficient T lymphocytes. J. Exp. Med. 186, 941–953.

Nishina, H., Fischer, K.D., Radvanyi, L., Shahinian, A., Hakem, R., Rubie, E.A., Bernstein, A., Mak, T.W., Woodgett, J.R., Penninger, J.M., 1997b. Stress-signalling kinase Sek1 protects thymocytes from apoptosis mediated by CD95 and CD3. Nature 385, 350–353.

Nishina, H., Vaz, C., Billia, P., Nghiem, M., Sasaki, T., De la Pompa, J.L., Furlonger, K., Paiqe, C., Hui, C., Fischer, K.D., Kishimoto, H., Iwatsubo, T., Katada, T., Woodgett, J.R., Penninger, J.M., 1999. Defective liver formation and liver cell apoptosis in mice lacking the stress signaling kinase SEK1/MKK4. Development 126, 505–516.

Osumi-Yamashita, N., Ninomiya, Y., Eto, K., 1997. Mammalian craniofacial embryology in vitro. Int. J. Dev. Biol. 41, 187–194.

Patel, V.P., Lodish, H.F., 1987. A fibronectin matrix is required for differentiation of murine erythroleukemia cells into reticulocytes. J. Cell Biol. 105, 3105–3118.

Sasaki, K., Sonoda, Y., 2000. Histometrical and three-dimensional analyses of liver hematopoiesis in the mouse embryo. Arch. Histol. Cytol. 63, 137–146.

Sasaki, T., Mizuochi, C., Horio, Y., Nakao, K., Akashi, K., Sugiyama, D., 2010. Regulation of hematopoietic cell clusters in the placental niche through SCF/Kit signaling in embryonic mouse. Development 137, 3941–3952.

Shi, Y., Massague, J., 2003. Mechanisms of TGF-signaling from cell membrane to the nucleus. Cell 113, 685–700.

Shull, M.M., Ormsby, I., Kier, A.B., Pawlowski, S., Diebold, R.J., Yin, M., Allen, R., Sidman, C., Proetzel, G., Calvin, D., Annunziata, N., Doetschman, T., 1992. Targeted disruption of the mouse transforming growth factor-b1 gene results in multifocal inflammatory disease. Nature 359, 693–699.

Strobel, E.S., Möbest, D., von Kleist, S., Dangel, M., Ries, S., Mertelsmann, R., Henschler, R., 1997. Adhesion and migration are differentially regulated in hematopoietic progenitor cells by cytokines and extracellular matrix. Blood 90, 3524–3532.

Sugiyama, D., Tsuji, K., 2006. Definitive hematopoiesis from endothelial cells in the mouse embryo; a simple guide. Trends Cardiovasc. Med. 16, 45–49.
Sugiyama, D., Arai, K., Tsuji, K., 2005. Definitive hematopoiesis from acetyl LDL incorporating endothelial cells in the mouse embryo. Stem Cells Dev. 14, 687–696.
Sugiyama, D., Kulkeaw, K., Mizuochi, C., Horio, Y., Okayama, S., 2011. Hepatoblasts comprise a niche for fetal liver erythropoiesis through cytokine production. Biochem. Biophys. Res. Commun. 410, 301–306.
Sugiyama, D., Ogawa, M., Hirose, I., Jaffredo, T., Arai, K., Tsuji, K., 2003. Erythropoiesis from acetyl LDL incorporating endothelial cells at the pre-liver stage. Blood 101, 4733–4738.
Suzuki, N., Suwabe, N., Ohneda, O., Obara, N., Imagawa, S., Pan, X., Motohashi, H., Yamamoto, M., 2003. Identification and characterization of 2 types of erythroid progenitors that express GATA-1 at distinct levels. Blood 102, 3575–3583.
Taipale, J., Keski-Oja, J., 1997. Growth factors in the extracellular matrix. FASEB J. 11, 51–59.
Tanimizu, N., Nishikawa, M., Saito, H., Tsujimura, T., Miyajima, A., 2003. Isolation of hepatoblasts based on the expression of Dlk/Pref-1. J. Cell Sci. 116, 1775–1786.
Taverna, D., Disatnik, M.H., Rayburn, H., Bronson, R.T., Yang, J., Rando, T.A., Hynes, R.O., 1998. Dystrophic muscle in mice chimeric for expression of alpha5 integrin. J. Cell Biol. 143, 849–859.
Tsai, S., Patel, V., Beaumont, E., Lodish, H.F., Nathan, D.G., Sieff, C.A., 1987. Differential binding of erythroid and myeloid progenitors to fibroblasts and fibronectin. Blood 69, 1587–1594.
Watabe, T., Nishihara, A., Mishima, K., Yamashita, J., Shimizu, K., Miyazawa, K., Nishikawa, S., Miyazono, K., 2003. TGF-beta receptor kinase inhibitor enhances growth and integrity of embryonic stem cell-derived endothelial cells. J. Cell Biol. 163, 1303–1311.
Watanabe, T., Nakagawa, K., Ohata, S., Kitagawa, D., Nishitai, G., Seo, J., Tanemura, S., Shimizu, N., Kishimoto, H., Wada, T., Aoki, J., Arai, H., Iwatsubo, T., Mochita, M., Watanabe, T., Satake, M., Ito, Y., Matsuyama, T., Mak, T.W., Penninger, J.M., Nishina, H., Katada, T., 2002. SEK1/MKK4-Mediated SAPK/JNK signaling participates in embryonic hepatoblast proliferation via a pathway different from NF-B-induced anti-apoptosis. Dev. Biol. 250, 332–347.
Williams, D.A., Rios, M., Stephens, C., Patel, P.V., 1991. Fibronectin and VLA-4 in haematopoietic stem cell-microenvironment interactions. Nature 352, 438–441.
Yanai, N., Sekine, C., Yagita, H., Obinata, M., 1994. Roles for integrin very late activation antigen-4 in stroma-dependent erythropoiesis. Blood 83, 2844–2850.
Yoshida, M., Nishikawa, Y., Omori, Y., Yoshioka, T., Tokairin, T., McCourt, P., Enomoto, K., 2007. Involvement of signaling of VEGF and TGF-beta in differentiation of sinusoidal endothelial cells during culture of fetal rat liver cells. Cell Tissue Res. 329, 273–282.
Zheng, X., Saunders, T.L., Camper, S.A., Samuelson, L.C., Ginsburg, D., 1995. Vitronectin is not essential for normal mammalian development and fertility. Proc. Natl. Acad. Sci. USA 92, 12426–12430.
Ziyadeh, F.N., Sharma, K., Ericksen, M., Wolf, G., 1994. Stimulation of collagen gene expression and protein synthesis in murine mesangial cells by high glucose is mediated by autocrine activation of transforming growth factor-beta. J. Clin. Invest. 93, 536–542.

OPEN ACCESS Freely available online

PLoS one

Intra-Aortic Clusters Undergo Endothelial to Hematopoietic Phenotypic Transition during Early Embryogenesis

Chiyo Mizuochi[1], Stuart T. Fraser[2], Katia Biasch[3], Yuka Horio[1], Yoshikane Kikushige[4], Kenzaburo Tani[5], Koichi Akashi[4], Manuela Tavian[3], Daisuke Sugiyama[1]*

1 Department of Hematopoietic Stem Cells,SSP Stem Cell Unit, Kyushu University Faculty of Medical Sciences, Fukuoka, Japan, **2** Laboratory of Blood Cell Development, Disciplines of Physiology, Anatomy and Histology, School of Medical Sciences, University of Sydney, Camperdown, New South Wales, Australia, **3** Unité 682 INSERM, Strasbourg, France, **4** Department of Medicine and Biosystemic Science, Kyushu University Graduate School of Medical Sciences, Fukuoka, Japan, **5** Department of Molecular Genetics, Medical Institute of Bioregulation, Kyushu University, Fukuoka, Japan

Abstract

Intra-aortic clusters (IACs) attach to floor of large arteries and are considered to have recently acquired hematopoietic stem cell (HSC)-potential in vertebrate early mid-gestation embryos. The formation and function of IACs is poorly understood. To address this issue, IACs were characterized by immunohistochemistry and flow cytometry in mouse embryos. Immunohistochemical analysis revealed that IACs simultaneously express the surface antigens CD31, CD34 and c-Kit. As embryos developed from 9.5 to 10.5 dpc, IACs up-regulate the hematopoietic markers CD41 and CD45 while down-regulating the endothelial surface antigen VE-cadherin/CD144, suggesting that IACs lose endothelial phenotype after 9.5 dpc. Analysis of the hematopoietic potential of IACs revealed a significant change in macrophage CFC activity from 9.5 to 10.5 dpc. To further characterize IACs, we isolated IACs based on CD45 expression. Correspondingly, the expression of hematopoietic transcription factors in the CD45(neg) fraction of IACs was significantly up-regulated. These results suggest that the transition from endothelial to hematopoietic phenotype of IACs occurs after 9.5 dpc.

Citation: Mizuochi C, Fraser ST, Biasch K, Horio Y, Kikushige Y, et al. (2012) Intra-Aortic Clusters Undergo Endothelial to Hematopoietic Phenotypic Transition during Early Embryogenesis. PLoS ONE 7(4): e35763. doi:10.1371/journal.pone.0035763

Editor: Alfons Navarro, University of Barcelona, Spain

Received March 3, 2011; **Accepted** March 22, 2012; **Published** April 27, 2012

Funding: This research was supported in part by the Project for Realization of Regenerative Medicine, Special Coordination Funds for Promoting Science and Technology of the Ministry of Education, Science, Sports and Culture (www.mext.go.jp/english); and SAKURA program of the Japan Society for the Promotion of Science (www.jsps.go.jp/english/index.html). The funders had no role in study design, data collection and analysis, decision to publish, or preparation of the manuscript.

Competing Interests: The authors have declared that no competing interests exist.

* E-mail: ds-mons@yb3.so-net.ne.jp

Introduction

During mouse embryogenesis, hematopoiesis begins at the extra-embryonic yolk sac (YS) at 7.5 days post-coitum (dpc) and shifts to fetal liver after mid-gestation, then to spleen and finally to bone marrow shortly before birth. There are two distinct waves of hematopoietic emergence: a transient wave, primarily restricted to erythropoiesis in YS blood islands prior to the connection of the circulation from the YS to the embryo; and a definitive wave originating in both the YS and embryo proper. The embryonic site has been identified in the aortic region, in the para-aortic splanchnopleura (p-Sp)/aorta-gonad-mesonephros (AGM) region [1–6]. Functional hematopoietic stem cells (HSCs) that can reconstitute adult recipients are first identified in the AGM region at 10.5 dpc after ex vivo organ culture [7]. The cells at 10.5 dpc that were not cultured ex vivo rarely reconstitute adult recipients, whereas those at 11.5 dpc can regardless [7–9]. Therefore, the cells that acquire HSC activity after culture step, have been termed "pre-HSC"s. Although several reports characterize the surface marker expression on both pre-HSCs at 10.5 dpc and HSCs at 11.5 dpc, the developmental process of HSC generation still remains unclear [8–11]. Cell populations capable of reconstituting neonatal recipients are detected in the p-Sp/AGM region at 9.5 dpc [12–13]. These observations suggest that ancestor cells of HSC from the p-Sp/AGM region at 9.5 dpc require special microenvironments to acquire HSC activity and that HSCs undergo phenotypic changes from 9.5 to 10.5 dpc. In the AGM region, intra-aortic/arterial clusters (IACs) are observed attached to floors of large arteries in several species including chicken, mouse and humans [3]. Mouse IACs have been characterized morphologically and are primarily located in three large arteries, namely, the dorsal aorta (DA), the omphalomesenteric (vitelline) artery (OMA; VA) and the umbilical artery (UA) [3,14–15]. IACs express both hematopoietic (CD41 and CD45) and endothelial (CD31, CD34 and VE-cadherin) surface markers [3,15–16] suggesting that IACs are likely equivalent to ancestor cells of HSC and/or pre-HSCs and are derived from endothelial cells (ECs) at aortic/arterial regions. Although recent genetic approaches and novel tracing methods demonstrate that IACs are derived from ECs in zebrafish and mice, it is unclear how IACs form and acquire HSC activity [17–25].

To address how IACs form and function in HSC generation, we first visualized IACs by immunohistochemistry and confocal imaging and were found to simultaneously express CD31, CD34 and c-Kit. This approach enabled us to investigate the phenotypic

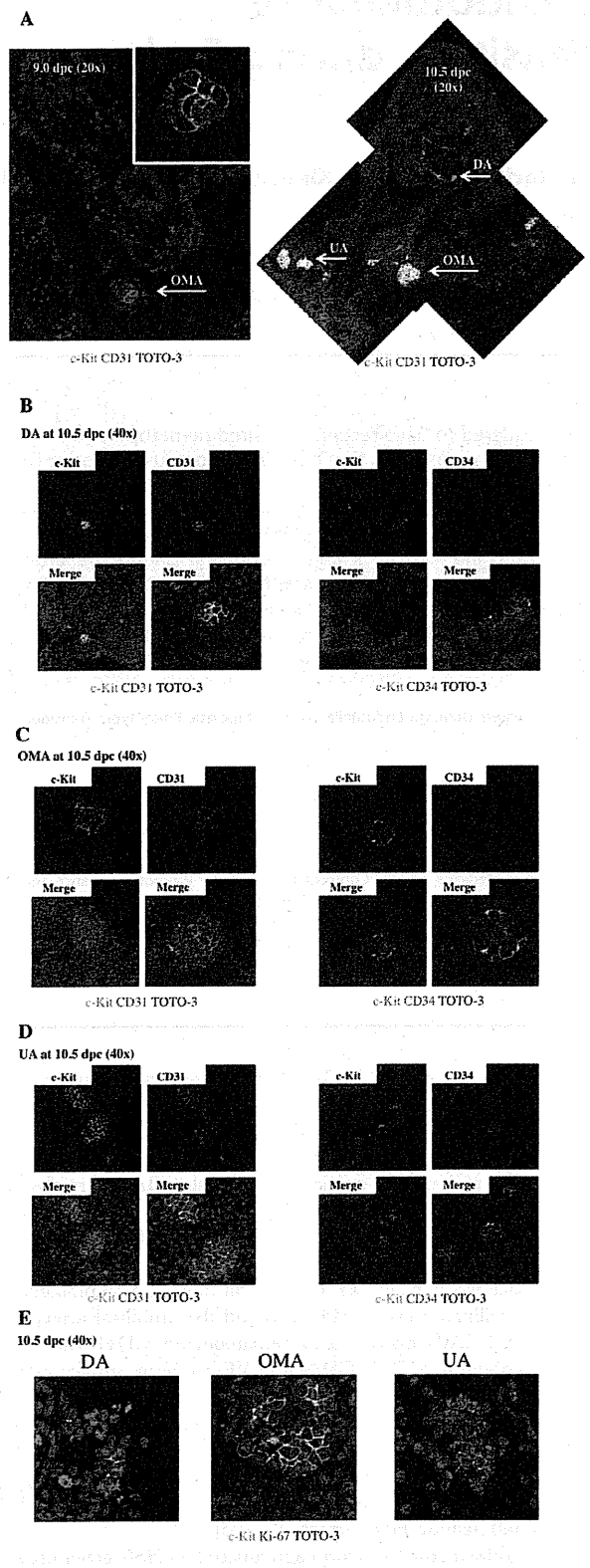

Figure 1. Confocal images of IACs expressing CD31/CD34/c-Kit in the AGM region. Transverse sections of AGM region from ICR mouse embryos at 9.0 and 10.5 dpc were stained with antibodies and observed by confocal microscopy. (**A**) IACs were observed in the omphalomesenteric artery (OMA) at 9.0 dpc (left; magnified view of IACs in upper right panel) and in the OMA, dorsal aorta (DA) and umbilical artery (UA) at 10.5 dpc (right). CD31 (red), c-Kit (green), and TOTO-3 (blue). Arrows indicate IACs. Original magnification is 20x. (**B-D**) IACs were observed in the DA (B), OMA (C) and UA (D) at 10.5 dpc. Left panel shows staining for CD31 (red), c-Kit (green), and TOTO-3 (blue), and right panel shows staining for CD34 (red), c-Kit (green), and TOTO-3 (blue) staining. Images were taken at 40x and zoom was used to show a detail at right lower panel. Another IAC in the DA is shown in Figure S1. (**E**) IACs expressing Ki-67, a marker of proliferation, were observed in the DA (left), OMA (middle) and UA (right). Ki-67 (red), c-Kit (green), and TOTO-3 (blue). Images were taken at 40x and zoom was used to show a detail.
doi:10.1371/journal.pone.0035763.g001

characterization of IACs by flow cytometry and hematopoiesis assays. Here, we demonstrate a significant transition from endothelial to hematopoietic cell phenotype of IAC cells after 9.5 dpc.

Results

Visualization of IACs in mouse embryos

Previous studies identified intra-aortic/arterial clusters (IACs) primarily by immunocytochemistry and microscopy [3,14–15]. Recently, we successfully visualized hematopoietic cell clusters in mouse placenta using thick (20 μm) cryo-sections and antibodies recognizing the embryonic HSC markers c-Kit, CD31 and CD34 and applied this method to quantifying IACs [26]. Cell aggregates consisting of more than three c-Kit-positive cells were defined as an IAC. Here, we used confocal microscopy to expand upon our previous study and characterize the cell types found within IACs according to c-Kit, CD31 and CD34 expression (Figure 1). The first IACs were observed as spherical structures in the omphalomesentric artery (OMA) at 9.0 dpc (12–14 somite pairs [SP]) (Figure 1A, left). Between 9.5 dpc (18–22 SP) to 10.5 dpc (30–34 SP), large arteries such as the dorsal aorta (DA), OMA and umbilical artery (UA) form [14]. IACs were observed in DA, OMA and UA at 10.5 dpc, and the size of IACs in the OMA and UA was significantly larger than those seen in the DA (Figure 1A, right). Localization of IACs in DA was not restricted to the ventral wall of DA, but rather some IACs were observed at dorsal and lateral sides of the wall (data not shown). All IACs in the DA, OMA and UA at 10.5 dpc simultaneously expressed c-Kit, CD31 and CD34 (Figure 1B-D). IACs expressing c-Kit in the different arteries analyzed were also positive for Ki-67, a marker of cell proliferation, regardless of location, suggesting that cells within IACs are highly proliferative (Figure 1E).

Characterization of IACs by flow cytometry and hematopoietic progenitor assays

To further characterize IACs, the caudal portion of embryos containing the p-Sp/AGM region was dissociated and analyzed by flow cytometry. At 10.5 dpc, c-Kit$^+$/CD31$^+$/CD34$^+$ cells, which are equivalent to IACs, were assessed for expression of the cell surface markers VE-cadherin/CD144 (an endothelial cell marker), CD41 (the earliest hematopoietic cell marker), CD45 (a pan-leukocyte marker), Sca-1 (a late fetal and adult HSC marker) and CD150 and EPCR (adult HSC markers) (Figure 2A-H). c-Kit$^+$/CD31$^+$/CD34$^+$ cells represented 0.069±0.01% in whole caudal portion of embryos. Among c-Kit$^+$/CD31$^+$/CD34$^+$ cells, VE-cadherin surface antigen expression decreased significantly within 24 hours from 9.5 to 10.5 dpc. Concomitantly, expression of the hematopoietic markers CD41 and CD45 increased from negative or low levels of expression on IAC cells at 9.5 dpc to abundant

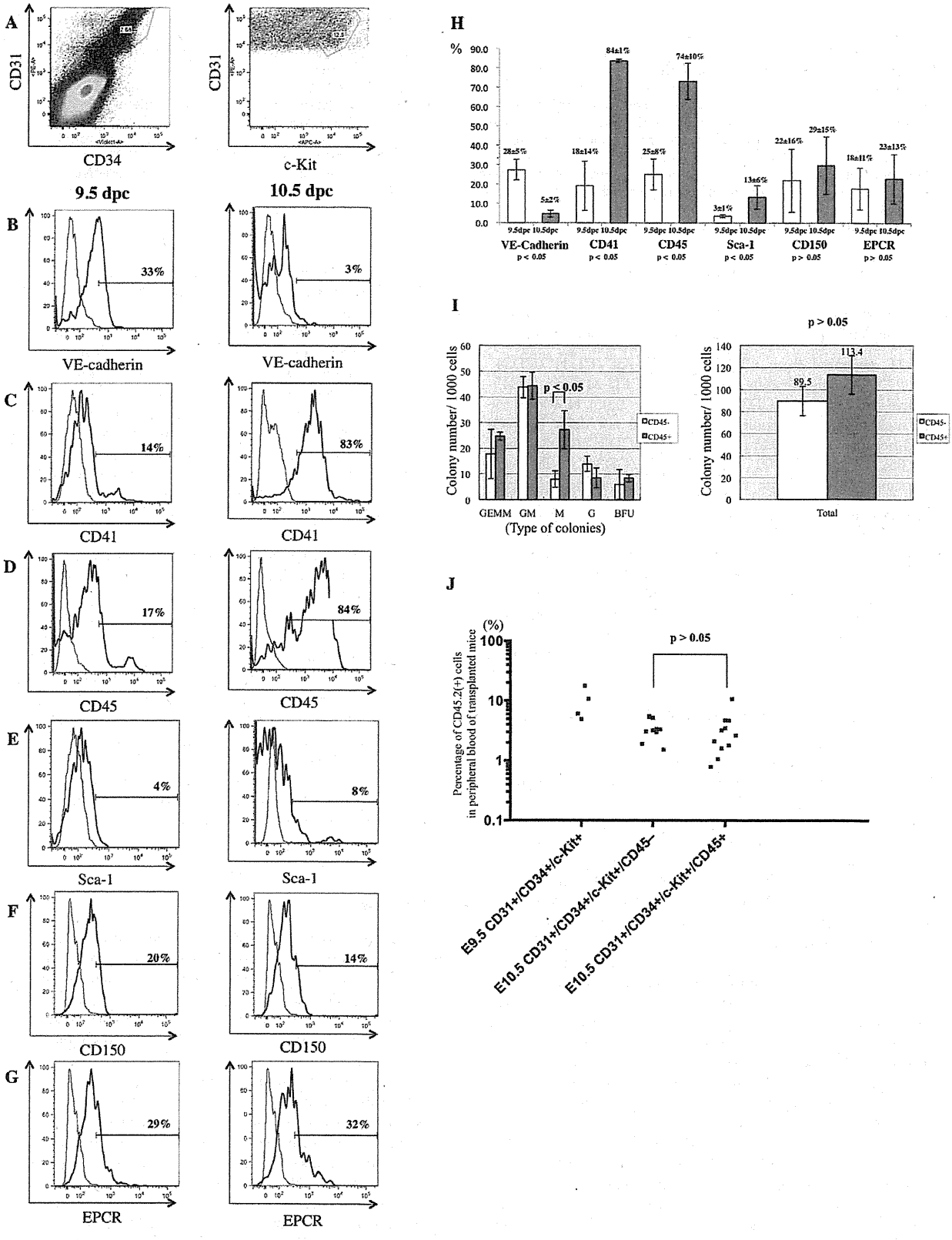

Figure 2. Flow cytometric analysis of CD31$^+$/CD34$^+$/c-Kit$^+$ AGM cells using surface expression of hematopoietic and endothelial cell markers. Single cell suspensions of the caudal portion of embryos containing the p-Sp/AGM region at 9.5 and 10.5 dpc were prepared and analyzed by flow cytometry. (**A**) Cells expressing CD31, CD34 and c-Kit markers of IACs were gated first. Isotype control of flow cytometric analysis is shown in

Figure S2. (**B-G**) Expression of hematopoietic and endothelial cell markers was analyzed on CD31$^+$/CD34$^+$/c-Kit$^+$ cells at 9.5 dpc (left) and 10.5 dpc (right) with the following antibodies: (**B**) VE-cadherin/CD144 (an endothelial cell marker), (**C**) CD41 (the earliest hematopoietic cell marker), (**D**) CD45 (a pan-leukocyte marker), (**E**) Sca-1 (a late fetal and adult HSC marker), (**F**) CD150 and (**G**) EPCR (adult HSC markers). At least 1,000 cells were assessed for each surface antigen. Representative profiles are shown. (**H**) Percentage of expression was summarized. At least 3 independent experiments were performed. Mean ± 2SD was calculated and shown at the top of bars. (**I**) One thousand sorted CD45-negative or CD45-positive CD31$^+$/CD34$^+$/c-Kit$^+$ cells were cultured in semisolid medium containing the hematopoietic cytokines, SCF (Stem Cell Factor), IL (Interleukin)-3, IL-6 and EPO (Erythropoietin). Left and right panels show each fraction and the total number of colonies, respectively. GEMM (colony-forming units of granulocyte erythrocyte monocyte macrophages); GM (of granulocyte macrophages); M (of macrophages); G (of granulocytes); BFU (burst forming units of erythroid cells). (**J**) 50–100 sorted CD31$^+$/CD34$^+$/c-Kit$^+$ cells at 9.5 dpc, as well as CD45-negative and CD45-positive CD31$^+$/CD34$^+$/c-Kit$^+$ cells were transplanted into busulfan-treated Ly5.1 mouse neonates. Approximately one year after transplantation, blood samples were collected and analyzed for CD45.2 expression by flow cytometry. Representative profile of flow cytometric analysis and its negative and positive controls are shown in Figure S3 and S6, respectively.
doi:10.1371/journal.pone.0035763.g002

levels at 10.5 dpc. Sca-1 expression also increased from 9.5 to 10.5 dpc.

We next separated c-Kit$^+$/CD31$^+$/CD34$^+$ cells based on CD45 expression by flow cytometry and performed colony assays and transplantation assays. As shown in Figure 2I (left), the number of CFU-M generated from CD45-positive c-Kit$^+$/CD31$^+$/CD34$^+$ cells (27.3) was significantly higher than CFU-M from CD45-negative c-Kit$^+$/CD31$^+$/CD34$^+$ cells (8.0) ($p<0.05$). However, the total number of hematopoietic colonies did not differ between CD45-negative and CD45-positive c-Kit$^+$/CD31$^+$/CD34$^+$ cells ($p>0.05$). When 50–100 c-Kit$^+$/CD31$^+$/CD34$^+$ cells were transplanted into neonate recipients, there was no significant difference in reconstitution ability (CD45-negative, 3.55%; CD45-positive 3.07%) ($p>0.05$) (Figure 2J). c-Kit$^+$/CD31$^+$/CD34$^+$ cells at 9.5 dpc were able to reconstitute recipients and chimerism to 9.89% was achieved. Presumptive ancestor cells of HSC can reportedly reconstitute neonate recipients but not adult recipients [13]. In addition, pre-HSCs at 10.5 dpc rarely reconstitute adult recipients without culture step [7–9,11]. When 100 c-Kit$^+$/CD31$^+$/CD34$^+$ cells were transplanted into adult recipients, no reconstitution was observed (data not shown).

Expression of CD45 in mouse and human intra-aortic/arterial clusters

CD45-negative and CD45-positive c-Kit$^+$/CD31$^+$/CD34$^+$ cells showed no difference in hematopoietic potential except within the macrophage lineage. To further investigate a role of CD45 expression on c-Kit$^+$/CD31$^+$/CD34$^+$ cells, we used flow cytometry to segregate c-Kit$^+$/CD31$^+$/CD34$^+$ cells into three fractions. Three distinct populations became apparent; CD45negative cells, CD45low cells, and CD45high cells (Figure 3A). The proportion of CD45-negative and CD45-low positive c-Kit$^+$/CD31$^+$/CD34$^+$ cells was higher at 9.5 dpc than at 10.5 dpc, whereas the percentage of CD45-high positive c-Kit$^+$/CD31$^+$/CD34$^+$ cells increased by 5-fold at 10.5 dpc (31.0%) compared to 9.5 dpc (6.3%) (Figure 3B). These data suggest that CD45-negative c-Kit$^+$/CD31$^+$/CD34$^+$ cells are precursors of CD45-high positive c-Kit$^+$/CD31$^+$/CD34$^+$ cells and that CD45 is a marker of IAC maturation. To address this issue, we examined expression levels of the gene encoding CD45 (*Ptprc; protein tyrosine phosphatase, receptor type, C*) and of various hematopoietic transcription factors (Runx1, c-Myb, Evi-1, SCL and Gata2) (Figure 3C-H). CD45-negative c-Kit$^+$/CD31$^+$/CD34$^+$ cells expressed low levels of *CD45* mRNA. *Ptprc* transcript levels increased significantly as CD45 surface protein expression was up-regulated in the c-Kit$^+$/CD31$^+$/CD34$^+$ population. Expression levels of all hematopoietic transcription factor genes assayed except *Evi-1* was highest in CD45-low positive c-Kit$^+$/CD31$^+$/CD34$^+$ cells. In agreement with flow cytometric analysis, evaluation of CD45 protein expression by immunohistochemistry indicated that IACs in the OMA at 9.5 dpc were CD45-negative while some IACs in the DA, OMA and UA were CD45-positive by 10.5 dpc (Figure 4A-D).

IAC formation in the developing human embryo is poorly defined. Having defined the developmental progression of IAC in the mouse above, we next examined IAC morphology and phenotype in a 32 day-old human embryo. Immunohistochemistry of embryonic human cryosections was performed using anti-human CD34 and CD45 antibodies. As shown in Figure 4E, IACs can be detected in ventral wall of the dorsal aorta. CD34 was expressed by a wide range of vascular endothelial cells throughout the embryo. CD45 was restricted to round and in many cases clearly circulating cells. However, within the IAC observable on the ventral wall of the dorsal aorta, cells expressing both CD34 and CD45 can be seen. This reflects the expression pattern we have identified in embryonic mouse IACs.

Transcription factor hierarchy in IAC development

We next observed IAC formation by immunohistochemistry and flow cytometry in mouse embryos harboring mutations associated with aberrant embryonic hematopoiesis [27–32]. Immunohistochemical analysis of *Runx1*$^{-/-}$ embryos lacked IACs in the DA, OMA and UA. Flow cytometric analyses confirmed the absence of c-Kit$^+$/CD31$^+$/CD34$^+$ cells in *Runx1*$^{-/-}$ embryos compared to wild type embryos (Figure 5A-B). *Evi-1*$^{-/-}$ embryos also lacked IACs in the DA, OMA and UA by immunohistochemistry. However, a small frequency of c-Kit$^+$/CD31$^+$/CD34$^+$ cells could be detected by flow cytometry (Figure 5C). In *c-Myb*$^{-/-}$ embryos, IACs were observed at the DA, OMA and UA, and c-Kit$^+$/CD31$^+$/CD34$^+$ cells were also observed by flow cytometry (Figure 5D). Collectively, these results demonstrate that Runx1 is essential for IAC formation while Evi-1 appears to be playing a function downstream of Runx1 in this process.

Discussion

During embryogenesis, a unique cell biological shift takes places in which endothelial cells with adherens junctions detach from each other, alter gene expression and become hematopoietic cells. This process is limited both anatomically and temporally. We here demonstrated that the transition from endothelial to hematopoietic phenotype of IACs occurs from 9.5 dpc in the mouse embryo, earlier than previously described. Furthermore, we show that IACs are identifiable in the human embryo based on CD45 expression, implying that this process in mice is applicable to human.

Previously, we reported an immunohistochemistry visualization technique revealing hematopoietic cell clusters in placenta using thick (20 μm) cryo-sections and antibodies recognizing embryonic HSC markers [26]. Here, we applied this technique to obtain high quality confocal images of intra-aortic/arterial clusters (IACs) in the AGM region. We defined IACs as c-Kit$^+$/CD31$^+$/CD34$^+$ cells. Recently, c-Kit$^+$/CD31$^+$/SSEA-1$^-$ cells were also identified in the AGM region [11]. As CD31 is expressed on both IACs and primordial germ cells (PGCs), it was necessary to exclude PGCs according to SSEA-1 expression. As shown in Figure 2 and 5, we

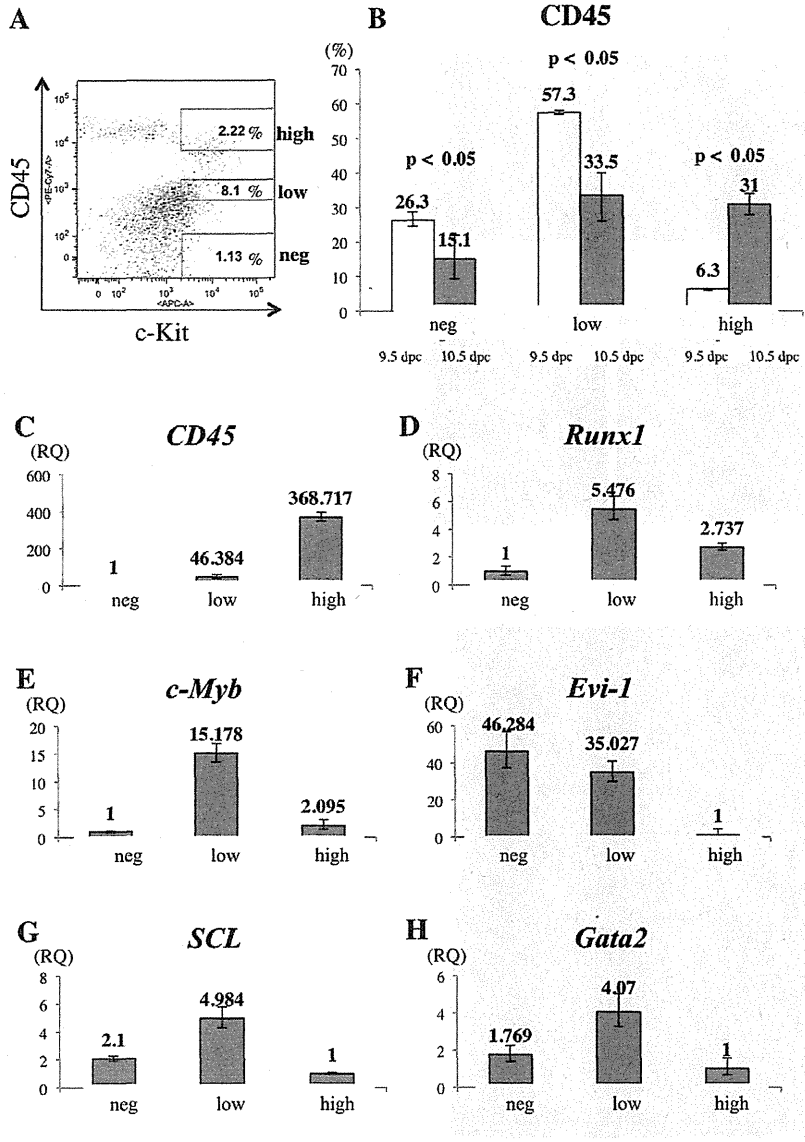

Figure 3. Gene expression analysis in CD31$^+$/CD34$^+$/c-Kit$^+$ AGM cells separated by CD45 expression. (**A**) Single cell suspensions of the caudal portion of embryos containing the AGM region at 10.5 dpc were prepared and analyzed by flow cytometry. Cells expressing CD31 and CD34, IAC markers, were first gated. The profile shows expression of c-Kit (x-axis) and CD45 (y-axis) in CD31$^+$/CD34$^+$ AGM cells (left). Based on intensity of CD45 expression, CD31$^+$/CD34$^+$/c-Kit$^+$ AGM cells were separated into three fractions, CD45-negative (under 10^2 of CD45-fluorescence, same as negative control), -low positive (from $10^{2.5}$ to $10^{3.5}$ of CD45-fluorescence), and -high positive (approximately over 10^4 of CD45-fluorescence). Isotype control and compensation samples of flow cytometric analysis are shown in Figure S4 and S5. (**B**) The percentage of CD45-negative, -low positive, and -high positive c-Kit$^+$/CD31$^+$/CD34$^+$ AGM cells was calculated both at 9.5 dpc (white bars) and 10.5 dpc (black bars). (**C-H**) Gene expression of *CD45* (C), *Runx1* (D), *c-Myb* (E), *Evi-1* (F), *SCL* (G) and *Gata2* (H) was analyzed in sorted CD45-negative, -low positive and -high positive c-Kit$^+$/CD31$^+$/CD34$^+$ AGM cells. Expression levels of *CD45* mRNA are up-regulated as c-Kit$^+$/CD31$^+$/CD34$^+$ cells express CD45 surface protein. Expression levels of *Runx1*, *c-Myb*, *Evi-1*, *SCL* and *Gata2* were highest in CD45-low positive c-Kit$^+$/CD31$^+$/CD34$^+$ cells, whereas that of *Evi-1* was highest in CD45-negative c-Kit$^+$/CD31$^+$/CD34$^+$ cells. RQ represents relative quantity of template in the original sample.
doi:10.1371/journal.pone.0035763.g003

could observe a small number of CD31$^+$/CD34$^-$ cells, which are likely to be PGCs. Since PGCs do not express CD34 at this stage, we could positively select the IAC fraction based on our definition by flow cytometry [33]. Our observation of IACs is compatible with the result showing large IACs were primarily observed in omphalomesentric artery (OMA) and umbilical artery (UA) at 10.5 dpc [11]. In the mouse, IACs protruding into the lumen of arteries were previously reported at 9.5 dpc in studies using microscopy and Tie-2 immunohistochemistry [14,34]. Prior to 9.5 dpc, we identified the first IACs, which formed a spherical structure, in the OMA at 9.0 dpc (Figure 1A). The OMA appears at 8.0 dpc and directly connects with the dorsal aorta (DA). The OMA anastomoses with the DA after 9.5 dpc and loses its connection with the UA by 10.5 dpc [14,35]. Our data (Figure 1E) indicate that IACs are proliferative, based on Ki-67 staining. Taken together, it is likely that the first IACs in the OMA proliferate and are distributed into

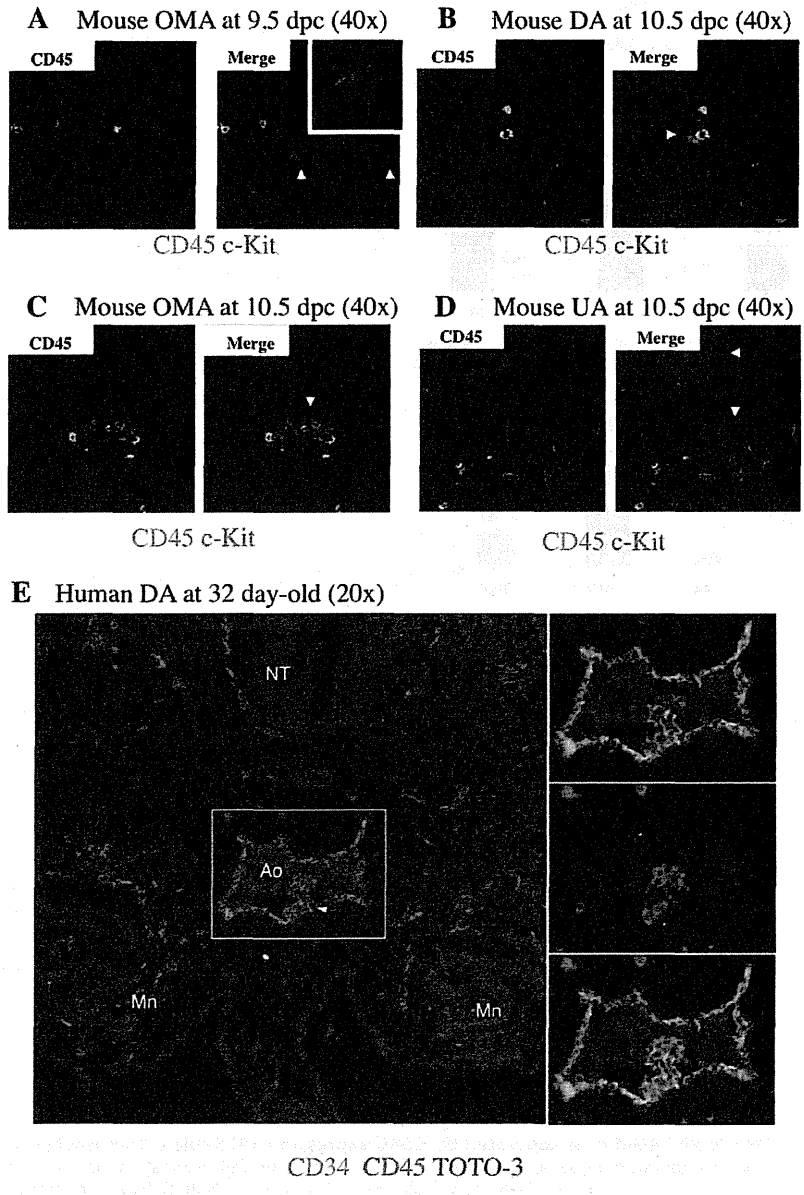

Figure 4. Expression of CD45 by mouse and human IACs. Transverse sections of AGM region were made from ICR mouse embryos at 9.5 and 10.5 dpc and from human embryos at 32 day-old, according to the Carnegie classification, stained with antibodies and observed by confocal microscopy. Arrowheads indicate IACs. (**A**) Mouse IACs in the omphalomesenteric artery (OMA) at 9.5 dpc expressed c-Kit, but not CD45. CD45 (green) and c-Kit (red). Magnified view of IACs is shown at right upper panel in Merge panel. Original magnification is 40x. (**B-D**) Mouse IACs in the dorsal aorta (DA) (B), OMA (C) and umbilical artery (UA) (D) at 10.5 dpc expressed c-Kit, and some expressed CD45. CD45 (green) and c-Kit (red). Original magnification is 40x. (**E**) All human IACs in the DA expressed CD34, and some expressed CD45. CD34 (green), CD45 (red) and TOTO-3 (blue). NT (Neural Tube); Ao (Aorta); Mn (Mesonephros). Original magnification is 20x.
doi:10.1371/journal.pone.0035763.g004

large arteries, such as the DA and UA, as the arterial system develops. Although several reports provide direct evidence that endothelial cells (ECs) generate IACs, we cannot rule out the possibility that either mesodermal cells, the ancestors of hematopoietic cells, or so-called hemangioblasts, which give rise both to ECs and hematopoietic cells, generate IACs by another pathway [17–25]. When VE-cadherin$^+$/CD45$^-$ cells were sorted out from AGM regions at 10.5 dpc, and co-aggregated with OP9 stromal cells, these cells acquired HSC activity [8]. As embryos develop, VE-cadherin$^+$/CD45$^+$ cells from AGM regions at 11.5 dpc can reconstitute adult recipients without culture step, whereas both VE-cadherin$^+$/CD45$^{+/-}$ cells can after aggregation culture with OP9 stromal cells. It suggests that the transition from endothelial to hematopoietic phenotype in pre-HSCs occurs between 10.5 and 11.5 dpc. According to our flow cytometric analysis of IACs, the transition from endothelial to hematopoietic phenotype occurs after 9.5 dpc (Figure 2). Although we found that 33% of c-Kit$^+$/CD31$^+$/CD34$^+$ cells at 9.5 dpc express VE-cadherin, most IACs defined as

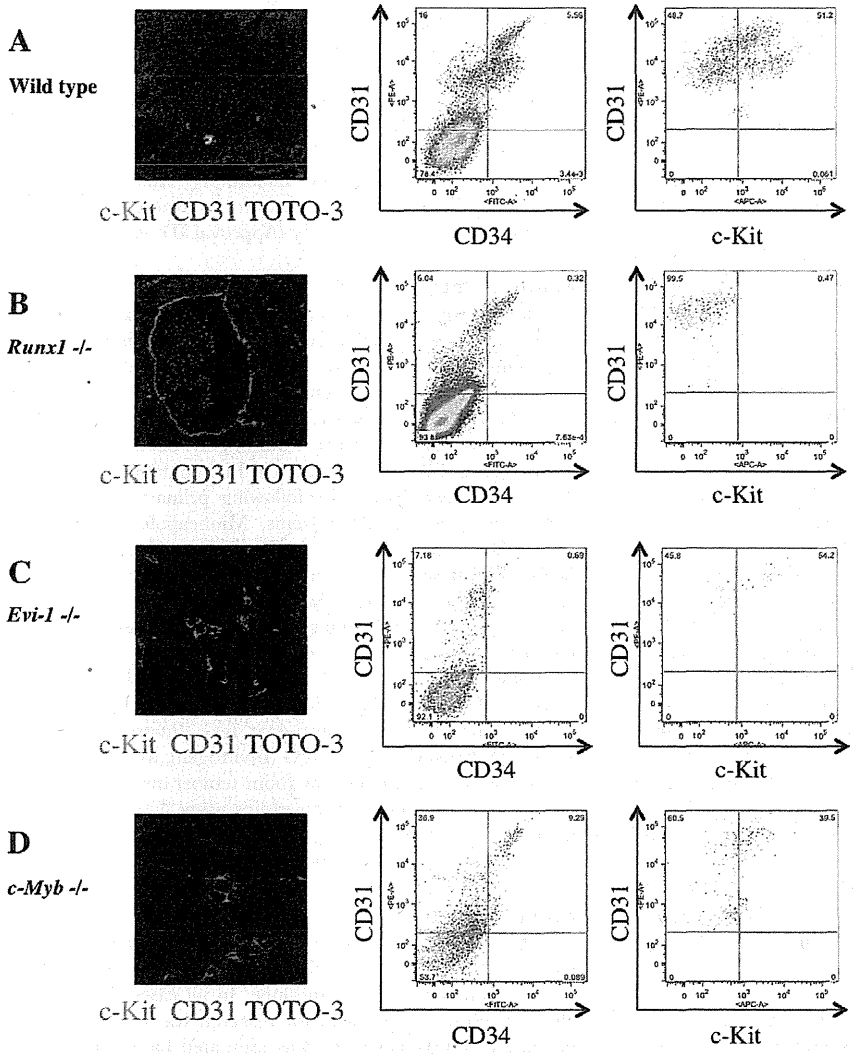

Figure 5. Altered IAC phenotype in *Runx1*$^{-/-}$, *Evi-1*$^{-/-}$ and *c-Myb*$^{-/-}$ embryos. Transverse sections of the AGM region were made from ICR, *Runx1*$^{-/-}$, *Evi-1*$^{-/-}$ and *c-Myb*$^{-/-}$ mouse embryos at 10.5 dpc, stained with antibodies and observed by confocal microscopy. Single cell suspensions of AGM regions from these embryos at 10.5 dpc were prepared and analyzed by flow cytometry. (**A-D**) Left panels show confocal images stained with anti-c-Kit (green) and CD31 (red) antibodies and TOTO-3 (blue). Middle and right panels show flow cytometric profiles of CD34 (x-axis) and CD31 (y-axis), and c-Kit (x-axis) and CD31 (y-axis), respectively. Isotype control and compensation samples of flow cytometric analysis are shown in Figure S2 and S5. (**A**) ICR mouse embryos serve as (wild type) controls. IACs and CD31^{+}/CD34^{+}/c-Kit^{+} AGM cells were observed. (**B**) No IACs were observed in *Runx1*$^{-/-}$ embryos, whereas the aortic structure was conserved (left). No CD31^{+}/CD34^{+}/c-Kit^{+} AGM cells were observed, whereas CD31^{+}/CD34^{+}/c-Kit^{-} AGM cells, which are equivalent to ECs, were observed (middle and right). (**C**) No IACs were observed and aortic structure was altered in *Evi-1*$^{-/-}$ embryos (left). CD31^{+} AGM cells were observed, but they did not express CD34 and c-Kit (middle and right). (**D**) IACs were observed in *c-Myb*$^{-/-}$ embryos and the aortic structure was conserved (left). CD31^{+}/CD34^{+}/c-Kit^{+} AGM cells were observed (middle and right).
doi:10.1371/journal.pone.0035763.g005

c-Kit^{+}/CD31^{+}/CD34^{+} cells by flow cytometry did not contribute to blood vessel structure. VE-cadherin is expressed in IACs as well as in ECs [16]. It is likely that sorted VE-cadherin^{+}/CD45^{-} cells from AGM regions at 10.5 dpc contained ECs with HSC potential in addition to some IACs. Further studies are necessary to determine how ECs contribute to IAC generation. CD150 belongs to the SLAM family and its expression is developmentally regulated on the surface of HSCs. At 11.5 dpc, CD150^{-} cells can reconstitute adult recipients, but CD150^{+} cells not [10]. In this study, CD150 expression was examined on c-Kit^{+}/CD31^{+}/CD34^{+} cells by flow cytometry and the percentage of CD150 expression was not changed (Figure 2F, H). It will be interesting to compare the CD150 expression between 10.5 and 11.5 dpc.

The pan-leukocyte marker CD45 is a transmembrane glycoprotein that functions as a protein phosphotyrosine phosphatase. Although loss of the *CD45* gene results in T and B lymphocyte anomalies in adult, there appears to be no significant abnormality in HSC development during embryogenesis [36–38]. We observed that CD45 protein expression was up-regulated in c-Kit^{+}/CD31^{+}/CD34^{+} cells between 9.5 and 10.5 dpc (Figure 2D). Our results are compatible with the report showing that CD45 is expressed on the surface of IACs at 10.5 dpc, but not on the IACs at 9.5 dpc [11].

In agreement with previous reports, we observed no significant differences in HSC activity based on neonatal transplantation, whereas myeloid potential differs based on colony formation assay between CD45-negative and CD45-positive c-Kit$^+$/CD31$^+$/CD34$^+$ cells, suggesting that CD45 expression is not required for hematopoietic cell identity (Figure 2I, J) [39–40]. However, pre-HSCs that can reconstitute both adult and neonatal recipients appear at 10.5 dpc, whereas presumptive ancestor cells of HSC that can reconstitute only neonatal but not adult recipients appear at 9.5 dpc [7,12–13]. In accordance with flow cytometric data, some IACs expressed CD45 while others did not in both 10.5 dpc mouse embryos and 32 day-old human embryos (Figure 4B-E). Taken together, although CD45 does not function in HSC development, its expression on the cell surface might serve as a marker of pre-HSC maturation from ancestor cells of HSC. With regard to myeloid potential, only macrophage development differs (Figure 2I). At 10.5 dpc, macrophages are reportedly c-Kit$^-$/CD31$^-$/CD45$^+$ cells, and we could observe some c-Kit$^-$/CD45$^+$ cells in the AGM regions (Figure 4) [11]. CD45 expression on c-Kit$^+$/CD31$^+$/CD34$^+$ cells might be the diverging point of myeloid potential. Furthermore, we identified *CD45* gene expression in CD45-negative c-Kit$^+$/CD31$^+$/CD34$^+$ cells, suggesting that these cells are primed to differentiate into CD45-positive c-Kit$^+$/CD31$^+$/CD34$^+$ cells. Expression levels of *Runx1, c-Myb, SCL* and *Gata2* were highest in CD45-low positive c-Kit$^+$/CD31$^+$/CD34$^+$ cells, implying that the transition from endothelial to hematopoietic phenotype of IACs occurs in CD45-low positive c-Kit$^+$/CD31$^+$/CD34$^+$ cells, as these transcription factors are reportedly important for the switch to hematopoietic cells [22]. Evi-1 is involved in vasculo-angiogenesis in addition to HSC development [31]. Therefore, high expression level of *Evi-1* gene in CD45-negative c-Kit$^+$/CD31$^+$/CD34$^+$ cells implies that this population still preserves some endothelial identity.

We also investigated IACs from *Runx1*$^{-/-}$, *Evi-1*$^{-/-}$ or *c-Myb*$^{-/-}$ mouse embryos. Runx1 is essential for definitive hematopoiesis, and its expression marks the site of *de novo* generation of definitive hematopoietic cells [28–30]. In agreement with previous reports, we observed an absence of IACs in *Runx1*$^{-/-}$ mouse embryos. *Evi-1*$^{-/-}$ mouse embryos displayed abnormalities in vascular and hematopoietic development [31–32]. As shown in Figure 5C, *Evi-1*$^{-/-}$ mouse embryos comprised a few c-Kit$^+$/CD31$^+$/CD34$^+$ cells based on flow cytometric analysis. High expression of *Evi-1* in CD45-negative c-Kit$^+$/CD31$^+$/CD34$^+$ cells may correlate with vascular development and impairment of IAC formation. c-Myb is essential for HSC maturation and proliferation, and *c-Myb*$^{-/-}$ mouse embryos die at 15.5 dpc from impaired definitive hematopoiesis in fetal liver, although primitive hematopoiesis appears normal [27]. In contrast to *Runx1*$^{-/-}$ or *Evi-1*$^{-/-}$ mouse embryos, *c-Myb*$^{-/-}$ mouse embryos exhibited IACs.

Several evidences reveal that HSCs are generated from ECs [17–21]. Taken together, our results corroborate HSC-generation from ECs and imply that IACs gradually acquire hematopoietic phenotype after 9.5 dpc. Understanding how IACs are generated could lead to an understanding of how to manipulate HSC generation from ES/iPS cells and thus be applicable to future clinical applications.

Materials and Methods

Mice

Ly5.1 (Sankyo Labo Service, Tokyo, Japan) mice, Ly5.2 adult C57/BL6 mice (Kyudo, Tosu, Japan), ICR mice (SLC, Hamamatsu, Japan), *Runx1*$^{+/-}$ mice (provided by Dr. Speck at University of Pennsylvania), *Evi-1*$^{+/-}$ mice (JAX mice and Services, Bar Harbor, ME) and *c-Myb*$^{+/-}$ mice (JAX mice and Services) were used in these studies. To analyze cells, pregnant mice were sacrificed at 9.0–10.5 dpc and somite pair number was counted. Embryos at 9.0 dpc with 12–14 somite pairs (SP), 9.5 dpc with 18–22 SP and 10.5 dpc with 30–34 SP were dissected out, respectively. Animals were handled according to the Guidelines for the Care and Use of Laboratory Animals of Kyushu University. This study was approved by Animal Care and Use Committee, Kyushu University (Approval ID: A21-068-0).

Mouse immunohistochemistry

Embryos were dissected out and fixed in 2% paraformaldehyde in PBS, followed by equilibration in 30% sucrose in PBS. Embryos were embedded in OCT compound (SAKURA, Tokyo, Japan) and frozen in liquid nitrogen. Tissues were sliced at 20 μm on a Leica CM1900 UV cryostat, transferred to glass slides (Matsunami, Osaka, Japan) and dried thoroughly. Sections were blocked in 1% BSA in PBS and incubated in PBS containing 1% BSA with appropriate dilutions of the following primary antibodies: goat anti-mouse c-Kit (R&D Systems, Minneapolis, MN), rat anti-mouse CD31 (BD Biosciences, San Diego, CA), rat anti-mouse CD34 (BD Biosciences), rat anti-mouse CD45 (Biolegend) and rat anti-mouse Ki-67 antigen (Dako Corporation, Carpinteria, CA) at 4̊C overnight. After washing in PBS three times, sections were incubated with appropriate dilutions of the following secondary antibodies: Alexa Fluor 488 donkey anti-rat IgG (Invitrogen, Carlsbad, CA), Alexa Fluor 488 donkey anti-goat IgG (Invitrogen), Alexa Fluor 546 donkey anti-goat IgG (Invitrogen) and Alexa Fluor 568 donkey anti-goat IgG (Invitrogen), as well as TOTO-3 (Invitrogen) to stain nuclei, at room temperature for 30 minutes. Samples were mounted on coverslips using fluorescent mounting medium (Dako Corporation) and assessed using a FluoView 1000 confocal microscope (Olympus, Tokyo, Japan).

Human tissues

Human embryos were obtained from voluntary abortions performed according to guidelines and with the approval of the French National Ethics Committee. In all cases, written consent allowing use of the embryo for research was obtained from the patient. Developmental age was estimated based on anatomical criteria and the Carnegie classification as previously described [41–42].

Human immunohistochemistry

Embryos were fixed overnight at 4°C in PBS plus 4% paraformaldehyde (Sigma-Aldrich), rinsed twice in PBS, then in PBS/15% sucrose (Sigma-Aldrich) for at least 24 hours. Tissues were then embedded in PBS with 15% sucrose and 7.5% gelatin (Sigma-Aldrich), frozen and stored at -80°C. Frozen sections (5 μm) were stored at −20°C until use, and then thawed and hydrated in PBS [37]. For double-staining, the TSA Plus Fluorescence amplification system was used, according to the manufacturer's instructions (NEN-Perkin Elmer). Endogenous peroxidases were inhibited for 20 minutes in PBS containing 0.2% hydrogen peroxide (Sigma-Aldrich). Sections were washed in PBS and non-specific binding sites were blocked with PBS/5% goat serum (Vector Laboratories) for 1 hour. Sections were then incubated with uncoupled antibody to CD45 (overnight at room temperature). After rinsing, sections were incubated with biotinylated goat anti-mouse IgG antibody (Immunotech) for 1 hour and then with peroxidase-labeled streptavidin (Immunotech) for 1 hour. Staining was revealed using fluorescent tyramide (TMR, Tetramethylrhodamine). Residual peroxidase activity was inhibited in PBS/0.2% hydrogen peroxide for 10 min at RT. After 3

washings in PBS, slides were treated with an Avidin/Biotin blocking kit according to the manufacturer's instructions (Vector Laboratories). Sections were washed and incubated with anti-CD34 antibody at room temperature for 2 hours, then with biotinylated goat anti-mouse IgG antibody (Immunotech) for 1 hour at RT, and with Alexa 488-labeled streptavidin for 1 hour. Slides were mounted in Vectashield medium (Vector Laboratories). Monoclonal antibodies to CD34 (IgG1, clone Qbend-10) and CD45 (IgG1, clone Hle-1) were purchased from Immunotech and Becton-Dickinson Biosciences, respectively.

Cell preparation

The caudal portion of embryos containing the p-Sp/AGM region was used to obtain a single cell suspension. Tissues were incubated with 1 mg/ml collagenase in medium supplemented with 10% fetal bovine serum for 30 minutes at 37°C and filtered through 40-μm nylon cell strainers (BD Biosciences).

Flow cytometry and cell sorting

Antibodies used for analysis were: FITC-conjugated anti-mouse CD41 (eBioscience, San Diego, CA), FITC-conjugated anti-mouse Sca-1 (eBioscience), FITC-conjugated anti-mouse EPCR (Endothelial Protein C Receptor) known as CD201 (Stem Cell Technologies inc, Vancouver, BC), PE-conjugated anti-mouse CD31 (BD Biosciences), PE-Cy7-conjugated anti-mouse CD45 (BioLegend), APC and APC-Cy7-conjugated anti-mouse c-Kit (BD Biosciences), Aexa Fluor488-conjugated anti-mouse CD150 (BioLegend), APC-conjugated anti-mouse VE-cadherin (clone name; VECD-1, provided by Dr. Ogawa at Kumamoto University), and FITC and Pacific Blue-conjugated anti-mouse CD34 (eBioscience). Flow cytometric analysis and cell sorting were carried out using a FACSAria SORP cell sorter (BDIS, San Jose, CA). Data files were analyzed using FlowJo software (Tree Star, Inc., San Carlos, CA).

RNA extraction and real-time PCR analysis

Total RNA was isolated using the RNAqueous 4PCR kit (Ambion Inc., Austin, Texas). mRNA was reverse transcribed using a High-Capacity RNA-to-cDNA kit (Life Technologies, Carlsbad, CA). The quality of cDNA synthesis was evaluated by amplifying mouse ß-actin using PCR. Thirty thermal cycles were used as follows: denaturation at 95°C for 10 sec, annealing at 60°C for 20 sec, followed by extension at 72°C for 20 seconds. Gene expression levels were measured by real time PCR with TaqMan® Gene Expression Master Mix and StepOnePlus™ real time PCR (Life Technologies). All probes were from TaqMan® Gene Expression Assays (Life Technologies). All analyses were performed in triplicate wells; mRNA levels were normalized to ß-actin and the relative quantity (RQ) of expression was compared with a reference sample.

Colony formation assay

Sorted cells were suspended in 3 ml of MethoCult® GF M3434 (Stemcell Technologies) distributed into three 35 mm dishes and then incubated in 5% CO_2 at 37°C. Colonies were counted up 14 days later using an inverted phase contrast microscope CKX41 (Olympus, Tokyo, Japan).

Transplantation assay

To examine neonatal repopulating HSCs, sorted cells were transplanted into busulfan-treated Ly5.1 mouse neonates as described previously [9,15]. Briefly, time-pregnant mice were injected on days 17 and 18 after conception with 15 μg of busulfan/gram body weight of the mother (Sigma-Aldrich, St.Louis MO). Isolated cells were suspended in 25 μl PBS and transplanted into neonates at the time of delivery using a 100 μl Hamilton syringe (Hamilton, Reno, NV). Approximately one year after transplantation, blood samples were collected, lysed in BD Pharm Lyse (BD Biosciences) and analyzed for CD45.2 expression by flow cytometry.

Supporting Information

Figure S1 Additional confocal images of IAC expressing CD31/CD34/c-Kit in the dorsal aorta of AGM region at 10.5 dpc. Staining for CD34 (red), c-Kit (green), and TOTO-3 (blue) is shown. Original magnification is 40x.
(TIFF)

Figure S2 Single cell suspensions of the caudal portion of embryos containing the p-Sp/AGM region at 9.5 and 10.5 dpc were prepared and analyzed by flow cytometry. Upper panels show isotype control of analysis corresponding to Figure 2A. Lower panels show isotype control of analysis corresponding to Figure 5.
(TIFF)

Figure S3 50–100 sorted $CD31^-/CD34^+/c\text{-}Kit^+$ cells at 9.5 dpc, as well as CD45-negative and CD45-positive $CD31^+/CD34^+/c\text{-}Kit^+$ cells were transplanted into busulfan-treated Ly5.1 mouse neonates. Approximately one year after transplantation, blood samples were collected, lysed in lysing solution and analyzed for CD45.2 expression by flow cytometry. Representative profile of flow cytometric analysis is shown.
(TIFF)

Figure S4 Single cell suspensions of the caudal portion of embryos containing the AGM region at 10.5 dpc were prepared and analyzed by flow cytometry. The profile shows isotype control of analysis corresponding to Figure 3A. Based on the isotype control, sorting gates are set into three fractions, CD45-negative (under 10^2 of CD45-fluorescence, same as negative control), -low positive (from $10^{2.5}$ to $10^{3.5}$ of CD45-fluorescence), and -high positive (approximately over 10^4 of CD45-fluorescence).
(TIFF)

Figure S5 Single cell suspensions of the caudal portion of embryos containing the p-Sp/AGM region at 9.5 and 10.5 dpc were prepared and analyzed by flow cytometry. Compensation samples of analysis corresponding to Figure 3A and 5 were shown.
(TIFF)

Figure S6 Negative and positive controls to transplantation analysis are shown corresponding to Figure S3. Peripheral blood samples were obtained from Ly5.1 adult mouse for negative control and Ly5.2 adult C57/BL6 mice for positive control, respectively.
(TIFF)

Acknowledgments

We thank the Research Support Center, the Graduate School of Medical Sciences, Kyushu University for technical support, Drs. K. Nakao and K. Kulkeaw for technical support, and Dr. Elise Lamar for critical reading of our manuscript.

Author Contributions

Conceived and designed the experiments: DS. Performed the experiments: CM KB YH YK MT DS. Analyzed the data: CM SF KB MT DS. Contributed reagents/materials/analysis tools: CM KB MT KT KA DS. Wrote the paper: CM SF DS.

References

1. Dzierzak E, Speck NA (2008) Of lineage and legacy: the development of *mammalian hematopoietic stem cells*. Nat Immunol 9: 129–136.
2. Mikkola HK, Orkin SH (2006) The journey of developing hematopoietic stem cells. Development 133: 3733–3744.
3. Godin I, Cumano A (2002) The hare and the tortoise: an embryonic haematopoietic race. Nat Rev Immunol 2: 593–604.
4. Dieterlen-Lievre F, Pouget C, Bollerot K, Jaffredo T (2006) Are intra-aortic hemopoietic cells derived from endothelial cells during ontogeny? Trends Cardiovasc Med 16: 128–139.
5. Jaffredo T, Bollerot K, Sugiyama D, Gautier R, Drevon C (2005) Tracing the hemangioblast during embryogenesis: developmental relationships between endothelial and hematopoietic cells. Int J Dev Biol 49: 269–277.
6. Sugiyama D, Tsuji K (2006) Definitive hematopoiesis from endothelial cells in the mouse embryo; a simple guide. Trends Cardiovasc Med 16: 45–49.
7. Medvinsky A, Dzierzak E (1996) Definitive hematopoiesis is autonomously initiated by the AGM region. Cell 86: 897–906.
8. Taoudi S, Gonneau C, Moore K, Sheridan JM, Blackburn CC, et al. (2008) Extensive hematopoietic stem cell generation in the AGM region via maturation of VE-cadherin+CD45+ pre-definitive HSCs. Cell Stem Cell 3: 99–108.
9. Rybtsov S, Sobiesiak M, Taoudi S, Souilhol C, Senserrich J, et al. (2011) Hierarchical organization and early hematopoietic specification of the developing HSC lineage in the AGM region. J Exp Med 208: 1305–1315.
10. McKinney-Freeman SL, Naveiras O, Yates F, Loewer S, Philitas M, et al. (2009) Surface antigen phenotypes of hematopoietic stem cells from embryos and murine embryonic stem cells. Blood 114: 268–278.
11. Yokomizo T, Dzierzak E (2010) Three-dimensional cartography of hematopoietic clusters in the vasculature of whole mouse embryos. Development 137: 3651–3661.
12. Kumano K, Chiba S, Kunisato A, Sata M, Saito T, et al. (2003) Notch1 but not Notch2 is essential for generating hematopoietic stem cells from endothelial cells. Immunity 18: 699–711.
13. Yoder MC, Hiatt K, Dutt P, Mukherjee P, Bodine DM, et al. (1997) Characterization of definitive lymphohematopoietic stem cells in the day 9 murine yolk sac. Immunity 7: 335–344.
14. Garcia-Porrero JA, Godin IE, Dieterlen-Lievre F (1995) Potential intraembryonic hemogenic sites at pre-liver stages in the mouse. Anat Embryol (Berl) 192: 425–435.
15. Garcia-Porrero JA, Manaia A, Jimeno J, Lasky LL, Dieterlen-Lievre F, et al. (1998) Antigenic profiles of endothelial and hemopoietic lineages in murine intraembryonic hemogenic sites. Dev Comp Immunol 22: 303–319.
16. Fraser ST, Ogawa M, Yokomizo T, Ito Y, Nishikawa S (2003) Putative intermediate precursor between hematogenic endothelial cells and blood cells in the developing embryo. Dev Growth Differ 45: 63–75.
17. Jaffredo T, Gautier R, Eichmann A, Dieterlen-Lievre F (1998) Intraaortic hemopoietic cells are derived from endothelial cells during ontogeny. Development 125: 4575–4583.
18. Sugiyama D, Ogawa M, Hirose I, Jaffredo T, Arai K, et al. (2003) Erythropoiesis from acetyl LDL incorporating endothelial cells at the preliver stage. Blood 101: 4733–4738.
19. Sugiyama D, Arai K, Tsuji K (2005) Definitive hematopoiesis from acetyl LDL incorporating endothelial cells in the mouse embryo. Stem Cells Dev 14: 687–696.
20. Bertrand JY, Giroux S, Golub R, Klaine M, Jalil A, et al. (2005) Characterization of purified intraembryonic hematopoietic stem cells as a tool to define their site of origin. Proc Natl Acad Sci U S A 102: 134–139.
21. Zovein AC, Hofmann JJ, Lynch M, French WJ, Turlo KA, et al. (2008) Fate tracing reveals the endothelial origin of hematopoietic stem cells. Cell Stem Cell 3: 625–636.
22. Chen MJ, Yokomizo T, Zeigler BM, Dzierzak E, Speck NA (2009) Runx1 is required for the endothelial to haematopoietic cell transition but not thereafter. Nature 457: 887–891.
23. Bertrand JY, Chi NC, Santoso B, Teng S, Stainier DY, et al. (2010) *Haematopoietic stem cells derive directly from aortic endothelium during* development. Nature 464: 108–111.
24. Kissa K, Herbomel P (2010) Blood stem cells emerge from aortic endothelium by a novel type of cell transition. Nature 464: 112–115.
25. Boisset JC, van Cappellen W, Andrieu-Soler C, Galjart N, Dzierzak E, et al. (2010) In vivo imaging of haematopoietic cells emerging from the mouse aortic endothelium. Nature 464: 116–120.
26. Sasaki T, Mizuochi C, Horio Y, Nakao K, Akashi K, et al. (2010) Regulation of hematopoietic cell clusters in the placental niche through SCF/Kit signaling in embryonic mouse. Development 137: 3941–3952.
27. Mucenski ML, McLain K, Kier AB, Swerdlow SH, Schreiner CM, et al. (1991) A functional c-myb gene is required for normal murine fetal hepatic hematopoiesis. Cell 65: 677–689.
28. Okuda T, van Deursen J, Hiebert SW, Grosveld G, Downing JR (1996) AML1, the target of multiple chromosomal translocations in human leukemia, is essential for normal fetal liver hematopoiesis. Cell 84: 321–330.
29. Wang Q, Stacy T, Binder M, Marin-Padilla M, Sharpe AH, et al. (1996) Disruption of the Cbfa2 gene causes necrosis and hemorrhaging in the central nervous system and blocks definitive hematopoiesis. Proc Natl Acad Sci U S A 93: 3444–3449.
30. North T, Gu TL, Stacy T, Wang Q, Howard L, et al. (1999) Cbfa2 is required for the formation of intra-aortic hematopoietic clusters. Development 126: 2563–2575.
31. Yuasa H, Oike Y, Iwama A, Nishikata I, Sugiyama D, et al. (2005) Oncogenic transcription factor Evi1 regulates hematopoietic stem cell proliferation through GATA-2 expression. EMBO J 24: 1976–1987.
32. Goyama S, Yamamoto G, Shimabe M, Sato T, Ichikawa M, et al. (2008) Evi-1 is a critical regulator for hematopoietic stem cells and transformed leukemic cells. Cell Stem Cell 3: 207–220.
33. Wood HB, May G, Healy L, Enver T, Morris-Kay GM (1997) CD34 expression patterns during early mouse development are related to modes of blood vessel formation and reveal additional sites of hematopoiesis. Blood 90: 2300–2311.
34. Takakura N, Huang XL, Naruse T, Hamaguchi I, Dumont DJ, et al. (1998) Critical role of the TIE2 endothelial cell receptor in the development of definitive hematopoiesis. Immunity 9: 677–686.
35. Theiler K (1972) The house mouse: development and normal stages from fertilization to 4 weeks of age. Springer, Berlin Heidelberg New York.
36. Kishihara K, Penninger J, Wallace VA, Kundig TM, Kawai K, et al. (1993) Normal B lymphocyte development but impaired T cell maturation in CD45-exon6 protein tyrosine phosphatase-deficient mice. Cell 74: 143–156.
37. Byth KF, Conroy LA, Howlett S, Smith AJ, May J, et al. (1996) CD45-null *transgenic mice reveal a positive regulatory role for CD45 in early thymocyte* development, in the selection of CD4+CD8+ thymocytes, and B cell maturation. J Exp Med 183: 1707–1718.
38. Mee PJ, Turner M, Basson MA, Costello PS, Zamoyska R, et al. (1999) Greatly reduced efficiency of both positive and negative selection of thymocytes in CD45 tyrosine phosphatase-deficient mice. Eur J Immunol 29: 2923–2933.
39. North TE, de Bruijn MF, Stacy T, Talebian L, Lind E, et al. (2002) Runx1 expression marks long-term repopulating hematopoietic stem cells in the midgestation mouse embryo. Immunity 16: 661–672.
40. Matsubara A, Iwama A, Yamazaki S, Furuta C, Hirasawa R, et al. (2005) Endomucin, a CD34-like sialomucin, marks hematopoietic stem cells throughout development. J Exp Med 202: 1483–1492.
41. O'Rahilly R, Muller F (1987) Development Stages in Human Embryos. Washington: Carnegie Institution of Washington.
42. Tavian M, Peault B (2005) The changing cellular environments of hematopoiesis in human development in utero. Exp Hematol 33: 1062–1069.

Cell Biology International

Cell Biol. Int. (2012) 36, 195–202 (Printed in Great Britain)

online data

Research Article

Ectopic expression of Hmgn2 antagonizes mouse erythroid differentiation *in vitro*

Kasem Kulkeaw*, Tomoko Inoue*,†, Chiyo Mizuochi*, Yuka Horio*, Yasushi Ishihama‡ and Daisuke Sugiyama[1]*

* Advanced Medical Initiatives, Division of Hematopoietic Stem Cells, Department of Advanced Medical Initiatives, Faculty of Medical Sciences, Kyushu University, Fukuoka, 812-8582, Japan

† Department of Molecular Genetics, Medical Institute of Bioregulation, Kyushu University, Fukuoka, 812-8582, Japan

‡ Graduate School of Pharmaceutical Sciences, Kyoto University, Kyoto, 606-8501, Japan

Abstract

Hmgn2 (high mobility group nucleosomal 2), a ubiquitous nucleosome-binding protein that unfolds chromatin fibres and enhances DNA replication, reportedly regulates differentiation of epithelial and mesenchymal cells. To investigate how Hmgn2 regulates HC (haemopoietic cell) differentiation, we quantified *Hmgn2* expression in HCs of mouse FL (fetal liver) during erythroid differentiation. *Hmgn2* expression levels were >10-fold higher in immature erythroid progenitors than in mature erythroid cells, suggesting that Hmgn2 antagonizes erythroid differentiation. To address this issue, *Hmgn2* were transfected into both Friend erythroleukaemia cells and FL HCs. There was a 3.3-fold decrease in relatively mature c-Kit$^+$/CD71$^+$ erythroid cells, a 2.9-fold increase in immature c-Kit$^+$/CD71$^-$ erythroid cells in transfected Friend cells, a 1.1-fold decrease in relatively mature CD71$^+$/Ter119$^+$ erythroid cells, and a 1.7-fold increase in relatively immature c-Kit$^+$/CD71$^+$ erythroid cells in FL HCs accompanied by down-regulation of genes encoding the erythroid transcription factors, Gata1 and Klf1. Two days after *Hmgn2* transfection of Friend erythroleukaemia cells, the number of S-phase cells increased, whereas the number of cells in G_1 decreased, while that of mitotic cells remained unchanged. We conclude that ectopic expression of Hmgn2 antagonizes mouse erythroid differentiation *in vitro*, which may be due to enhancement of DNA replication and/or blocking entry of mitosis at S-phase.

Keywords: erythroid differentiation; erythroleukaemia cell; fetal liver; Hmgn2

1. Introduction

Hmgn (high mobility group nucleosomal)-binding proteins constitute a family of ubiquitous nuclear proteins comprising Hmgn1–Hmgn4 and NSBP1 (nucleosomal binding protein 1). Hmgn1 and Hmgn2 are widely expressed, whereas the remaining family members have a more tissue-specific expression pattern (Bustin 1999, 2001). Nuclear Hmgn1 and Hmgn2, which are 53% homologous, constitute approximately 10% of all nuclear protein in mice (Bustin and Reeves, 1996). Both bind to nucleosomes as a homodimer. The NBD (nucleosome-binding domain) binds to the 147 bp nucleosome core particle rather than to a specific DNA sequence (Shirakawa et al., 2000; Ueda et al., 2008), while the CHUD (chromatin-unfolding domain) reduces compactness of the chromatin fibre (Bustin, 2001). Hmgn2 facilitates accessibility of transcription factors and the replication machinery to chromatin, thereby enhancing transcription (Trieschmann et al., 1995a, 1995b) and DNA replication (Vestner et al., 1998). In addition to nucleosome binding, Hmgn2 also modulates DNA binding of homeodomain transcription factors (Amen et al., 2008). At the 2-cell stage in mouse embryos, *Hmgn2* knockdown by antisense oligonucleotide delays cell division (Mohamed et al., 2001). *Hmgn2* expression is also down-regulated during differentiation of osteoblasts in mouse embryos (Shakoori et al., 1993). However, Hmgn2 is highly expressed in cells undergoing differentiation, such as the basal layer of epithelial cells in *Xenopus laevis* (Korner et al., 2003) and mesenchymal-to-epithelial transitions in the mouse kidney (Lehtonen and Lehtonen, 2001).

Haematopoiesis is the process in which HSCs (haemopoietic stem cells) are generated, differentiate into specific progenitors and mature into various blood cell types, such as erythrocytes, megakaryocytes, lymphocytes, neutrophils and macrophages (Weissman, 2000). Erythropoiesis is the process by which a large number of enucleated erythrocytes are produced from HSCs (McGrath and Palis, 2008). During embryogenesis, the FL (fetal liver) is a major organ of HSC expansion and erythrocyte production (Ema and Nakauchi, 2000; Sugiyama and Tsuji, 2006). Erythropoiesis shifts to BM (bone marrow) shortly before birth (Dzierzak et al., 1998). During erythroid differentiation, erythroblasts lose their capacity to proliferate and leave the cell cycle (Buttitta and Edgar, 2007). However, molecular mechanisms underlying erythroid differentiation have not been fully elucidated.

We have focused on the role of Hmgn2 in erythroid differentiation in mice. By assessing the differentiation status of erythroid cells by flow cytometry and gene expression after

[1] To whom correspondence should be addressed (email ds-mons@yb3.so-net.ne.jp).

Abbreviations: AcGFP, *Aequorea coerulescens* green fluorescent protein; APC, allophycocyanin; BFU-E, burst-forming unit-erythroid; CFU-E, colony-forming unit-erythroid; CHUD, chromatin-unfolding domain; dpc, day post coitum; EPO, erythropoietin; FBS, fetal bovine serum; FL, fetal liver; GFP, green fluorescent protein; HC, haemopoietic cell; Hmgn, high mobility group nucleosomal; HSC, haemopoietic stem cell; IL-3, interleukin 3; IRES, internal ribosome entry site; α-MEM, α-minimum essential medium; MNC, mononuclear cell; NBD, nucleosome-binding domain; NLS, nuclear localization signal; PE, phycoerythrin; PI, propidium iodide; PBSBA, BSA in PBS; RQ, relative quantity; RT–PCR, reverse transcription–PCR; Sca-1, stem cell antigen-1; SCF, stem cell factor; TBS-T, TBS containing 0.1% Tween-20; TPO, thrombopoietin; WB, Western blot.

ectopic expression of *Hmgn2* by electroporation, Hmgn2 is shown to antagonize erythroid differentiation of erythroleukaemia cells and mouse FL cells *in vitro*.

2. Materials and methods

2.1. Animals and cell lines

C57BL6J mice were purchased from Nihon SLC (Hamamatsu). Noon on the day of the plug was defined as 0.5 dpc (day post coitum). To analyse their cells, pregnant mice were killed and their embryos dissected out. Animals were handled according to the Guidelines for the Care and Use of Laboratory Animals of Kyushu University. This study was approved by Animal Care and Use Committee, Kyushu University (Approval ID: A21-068-0). The Friend erythroleukaemia cell line, F5-5.fl, was purchased from the RIKEN Bio-Resource Center. Cells were maintained in RPMI 1640 (Wako Pure Chemical Industries) containing 10% FBS (fetal bovine serum) and 10 units/ml penicillin and 10 mg/ml streptomycin (Sigma–Aldrich). Cells were passaged every 3–4 days.

2.2. Construction of an *Hmgn2* vector

A primer set was designed from the known mouse mRNA sequence (accession no. NM_016957). Full-length *Hmgn2* was amplified from mouse FL cDNA and ligated into the pIRES2-AcGFP (*Aequorea coerulescens* green fluorescent protein) vector (Clontech). *Hmgn2* was located upstream of an IRES (internal ribosome entry site), which was flanked downstream by cDNA encoding AcGFP (Supplementary Figure S2B available at http://www.cellbiolint.org/cbi/036/cbi0360195add.htm). *Hmgn2* sequence was confirmed by DNA sequencing. Endotoxin-free plasmid was prepared using the QIAGEN® Plasmid Midi kit (QIAGEN). The construct was introduced into $CaCl_2$-competent DH5α *Escherichia coli* by the heat shock method.

2.3. Preparation of FL MNCs (mononuclear cells)

At 12.5 dpc, embryonic blood cells were collected by disassociating FL on a 40 μm nylon mesh and washed once with PBS. MNCs were obtained after centrifugation with lympholyte solution (CEDARLANE Laboratories). MNCs were washed twice in PBS and cultured for 24 h in α-MEM (α-minimum essential medium) containing 10% FBS, 20 ng/ml each of SCF (stem cell factor) and TPO (thrombopoietin) (PEPROTECH) and 10 units/ml penicillin and 10 mg/ml streptomycin (Sigma–Aldrich). Floating cells were used for electroporation.

2.4. Electroporation and cell differentiation

Friend erythroleukaemia cells were collected after 24 h culture and washed twice with PBS. Cells were resuspended in Gene Pulser® electroporation buffer (Bio-Rad) at 5×10^6 cells/ml. The cell suspension (400 μl) was mixed with 8 μg of endotoxin-free pIRES2-*Hmgn2-AcGFP* or pIRES2-*AcGFP* (mock), transferred into an electroporation cuvette (0.4 cm gap) and placed on ice for 5 min. Cells were electroporated using a Gene Pulser MXCell™ Electroporator (Bio-Rad) at optimized conditions (200 volts, 2000 μF, 1000 Ω and 20 ms). They were cultured in RPMI 1640 containing 10% FBS without antibiotics for 48 h. GFP (green fluorescent protein)-expressing cells were collected using a FACS Aria cell sorter (BD Biosciences) and cultured in RPMI 1640 containing 10% FBS, 10 units/ml penicillin and 10 mg/ml streptomycin (Sigma–Aldrich) for 6 days.

For FL MNCs, cells were collected by gently pipetting and washing twice with PBS. Cells were electroporated as above. Optimal conditions for FL cells were 300 volts, 2000 μF, 1000 Ω and 20 ms. Cells were cultured with α-MEM containing 10% FBS, 20 ng/ml each of SCF and TPO (PEPROTECH) without antibiotics for 48 h. GFP^+ $CD71^+/Ter119^-$ cells were collected using a FACS Aria cell sorter (BD Biosciences) and cultured in α-MEM containing 10% FBS, 20 ng/ml each of SCF, IL-3 (interleukin 3) and EPO (erythropoietin) (PEPROTECH) with 10 units/ml penicillin and 10 mg/ml streptomycin.

2.5. Flow cytometry and cell sorting

To isolate HSCs and erythroid cells, cells were stained with a FITC-conjugated anti-mouse CD71 antibody (BD Biosciences), a PE (phycoerythrin)-conjugated anti-mouse Sca-1 (stem cell antigen-1) antibody (BD Biosciences), an APC (antigen-presenting cell)-conjugated anti-mouse c-Kit (CD117) antibody (BD Biosciences), a PE-Cy7-conjugated anti-mouse CD45 antibody (eBioscience) and an APC-Cy7-conjugated anti-mouse Ter119 antibody (eBioscience) (Hattangadi et al., 2010; Inoue et al., 2011). To analyse differentiation of erythroleukaemia and erythroid cells from FL, cells were stained with an APC-conjugated anti-mouse c-Kit (CD117) antibody (BD Biosciences), a PE-conjugated anti-mouse CD71 antibody (eBiosciences), and an APC-Cy7-conjugated anti-mouse Ter119 antibody (eBioscience). Dead cells were excluded by PI (propidium iodide) staining (Life Technologies). Cells were sorted in using a FACS Aria cell sorter (BD). Data files were analysed with FlowJo software (Tree Star Inc.).

2.6. Real-time PCR

RNA was extracted from sorted cells using RNAqueous-4PCR™ and RiboPure™ kits (Life Technologies). mRNA was reverse-transcribed using a high-capacity RNA-to-cDNA kit (Life Technologies). The quality of cDNA synthesis was checked by amplifying mouse β-actin by PCR. Thirty thermal cycles were as follows: denaturation at 95°C for 10 s, annealing at 60°C for 20 s and extension at 72°C for 20 s. Gene expression levels were evaluated using RT–PCR (reverse transcription–PCR) with a TaqMan® Gene Expression Master Mix and StepOnePlus™ RT–PCR machine (Life Technologies). All probes were from TaqMan® Gene Expression Assays (Life Technologies). Samples were taken in triplicate. mRNA levels were normalized to β-actin and the RQ (relative quantity) of expression was compared with a reference sample. Statistical comparisons of RQ values were calculated using a *t* test.

2.7. Antibody staining and confocal microscopy

HSCs and erythroid cells were isolated from FL at 12.5 dpc by flow cytometry as above. They were cytocentrifuged on to glass slides (Matsunami) using a Shandon Cytospin® 3 cytocentrifuge (Thermo Electron Corporation) at 450 rev./min for 7 min. After drying at 25°C, cells were fixed in 1% PFA (paraformaldehyde) in PBS at 4°C for 30 min and washed in PBS 3 times. After blocking with 1% BSA in PBS, cells were stained with a rabbit anti-mouse Hmgn2 polyclonal antibody (Chemicon International) overnight at 4°C. After three washes in PBS, cells were stained with Alexa Fluor® 488 goat anti-rabbit IgG (1:300) (Life Technologies) and TOTO®-3 iodide (642/660, Life Technologies). Samples were examined under a FV-1000 laser scanning confocal microscope (Olympus).

2.8. WB (Western blot) analysis

Protein was extracted from the sorted cells by using Qproteome® Mammalian Protein Prep Kit (Qiagen) and was quantified by using Quick Start™ Bradford Dye Reagent (Bio-Rad Laboratories). Then 5 μg of protein was run on 15% SDS-polyacrylamide gels concurrently with a pre-stained protein marker (Precision Plus Protein™ Standards, Bio-Rad Laboratories) using Laemmli buffer. Gels were trans-blotted on to a PVDF membrane (Immobilon®-P Transfer Membrane, Millipore Billerica). The PVDF membrane was blocked in 5% non-fat dried skimmed milk powder in TBS-T (TBS containing 0.1% Tween-20) at 25°C for 1 h, washed with TBS-T and reacted with 1:1000 rabbit anti-mouse Hmgn2 polyclonal antibody (Chemicon International) overnight at 4°C. The membrane was thoroughly washed and incubated in a solution of 1:1000 goat anti-rabbit IgG-HRP (horseradish peroxidase) conjugate (R&D Systems) at 25°C for 1 h. After washing, signals were visualized by soaking the membrane in substrate solution (Amersham™ ECL® Plus Western Blotting Detection System, GE Healthcare). Images were captured using ChemiDoc XRS (Bio-Rad Laboratories) and data were analysed by Quantity One ver. 4.6.7 (Bio-Rad Laboratories) and displayed as intensity per mm^2.

2.9. Cell cycle analysis

Cells were washed twice with PBS containing 2% FBS and resuspended in 300 μl PBS. They were permeabilized by adding 700 μl 100% ethanol pre-cooled to −20°C. After mixing by gentle inversion, the cell suspension was placed on ice overnight. Cells were collected by centrifugation at 4000 rev./min at 4°C for 2 min. To eliminate RNA, cells were incubated with 50 μl RNase A solution (100 μg/ml) at 37°C for 30 min. To stain DNA, cells were resuspended in 450 μl of staining solution containing 2 μg/ml PI (propidium iodide) in 100 mM Tris/HCl, pH 7.5, 150 mM NaCl, 1 mM $CaCl_2$, 0.5 mM $MgCl_2$ and 0.1% Nonidet P40, and incubated at 25°C for 30 min in the dark. Cells were analysed using a FACS Aria cell sorter (BD Biosciences). The percentages of cells in G_0+G_1 and in S+G_2 phases were calculated using the Watson Pragmatic method and FlowJo software.

2.10. Mitotic analysis by flow cytometry

Mitotic cell status was analysed as per Taylor (2004). Briefly, cells were washed twice in PBS, fixed in 70% ethanol at −20°C and resuspended in 400 μl PBS. Then 1 ml of cold ethanol (pre-cooled to −20°C) was added to the cell suspension, while gently vortexing the ethanol. The cells were fixed for at least 1 h at −20°C, transferred to a 1.5 ml Eppendorf tube and centrifuged at 3800 rev./min at 4°C for 7 min. After removal of supernatant by aspiration, the cell pellet was resuspended with 1 ml of PBS, centrifuged at 3800 rev./min at 4°C for 7 min, and the supernatant removed as above. The cell pellet was resuspended with 1.4 ml of PBS+0.25% Triton X-100 and incubated on ice for 15 min before being centrifuged at 3800 rev./min at 4°C for 7 min before the supernatant was removed. The cell pellet was resuspended in 100 μl 1% PBSBA (BSA in PBS) containing rabbit anti-phosphorylated histone H3 Ser^{10} IgG (Abcam) and incubated for 2 h at 25°C. Tubes were rocked gently for entire period. Then 1.3 ml of PBSBA was added, mixed by inverting and centrifuged at 3800 rev./min at 4°C for 7 min. After removal of the supernatant, the cell pellet was resuspended in 100 μl PBSBA containing Alexa Fluor® 647 goat anti-rabbit IgG (1:200) (Life Technologies) and incubated for 30 min at 25°C in the dark with gentle mixing as above. The cell suspension was washed once with 1.3 ml of PBSBA and centrifuged at 3800 rev./min at 4°C for 7 min. The cell pellet was resuspended in 500 μl of PBS containing 100 μg/ml DNase-free RNase A and incubated at 37°C for 30 min. After cooling on ice for a few seconds, 100 μl PI solution was added and incubated on ice for 15 min in the dark. Cells were analysed by flow cytometry.

2.11. Statistics

Student's *t* test in Microsoft Office Excel 2007 program was used to test a statistically significant differences ($P<0.05$) in the data.

3. Results

3.1. Expression of Hmgn2 in mouse FL during erythroid differentiation

Erythroid cell populations ranging from uncommitted HSCs to mature erythrocytes were sorted by flow cytometry from mouse FL at 12.5 dpc based on expression of the cell surface molecules CD45 (common leucocyte antigen), Sca-1, c-Kit (CD117, stem cell factor receptor), CD71 (transferrin receptor) and Ter119 (glycophorin) (Supplementary Figure S1A available at http://www.cellbiolint.org/cbi/036/cbi0360195add.htm). Erythroid cell populations were identified as follows: (i) the $CD45^+/Sca\text{-}1^+/c\text{-}Kit^+$ fraction defined HSCs; (ii) the $Sca\text{-}1^-/c\text{-}Kit^+/CD71^-/Ter119^-$ fraction defined BFU-E (burst-forming unit-erythroid); (iii) the $Sca\text{-}1^-/c\text{-}Kit^+/CD71^+/Ter119^-$ fraction defined committed erythroid progenitors or CFU-E (colony-forming unit-erythroid); (iv) the $Sca\text{-}1^-/c\text{-}Kit^-/CD71^+/Ter119^+$ fraction defined pro-erythroblasts; and (v) the $Sca\text{-}1^-/$

c-Kit$^-$/CD71$^-$/Ter119$^+$ fraction defined reticulocytes and erythrocytes (Supplementary Figures S1A and S1B).

To quantify *Hmgn2* expression levels during erythroid differentiation, RT–PCR analysis was carried out on each sorted population. *Hmgn2* expression levels increased slightly as HSCs differentiated into BFU-E (~1.4-fold, Figure 1A), but gradually decreased at later stages of erythroid cell differentiation (Figure 1A). *Hmgn2* expression in BFU-E and CFU-E was 14- and 12-fold higher than in mature erythrocytes, respectively ($P<0.05$; Figure 1A). Examining the expression of Hmgn2 protein by immunohistochemistry, single cell suspensions of HSCs, BFU-E, CFU-E, proerythroblasts and erythrocytes at 12.5 dpc were prepared, spun on to slides, stained with antibody to Hmgn2 and observed by confocal microscopy. Hmgn2 protein was expressed in all fractions (Figure 1B). To quantify the amount of Hmgn2 protein in each faction, WB analysis was used after loading the same amount of protein. Compatible with the immunohistochemistry data, Hmgn2 protein was detected in all fractions, the highest expression level being in the BFU-E fraction (Figure 1C).

3.2. Hmgn2 expression antagonizes erythroleukaemia cell differentiation

To investigate the function of Hmgn2 in erythroid differentiation, *Hmgn2* was ectopically expressed in Friend erythroleukaemia cells. Full-length mouse *Hmgn2* was cloned into an expression plasmid. The deduced amino acid sequence of Hmgn2 indicated 2 NLSs (nuclear localization signals; NLS1 and NLS2) in addition to the NBD and CHUD (Supplementary Figure S2A). Friend erythroleukaemia cells were transfected with plasmids with and without (mock) *Hmgn2* cDNA by electroporation. Two days later, expression levels of *Gata1* and *Klf1* that encode erythroid transcription factors were measured in transfected cells, identified by their GFP staining. Expression of *Gata1* and *Klf1* decreased in GFP$^+$ *Hmgn2*-transfected cells compared with mock controls ($P<0.05$; Figure 2A). However, expression levels of both *Gata1* and *Klf1* did not differ significantly between *Hmgn2*-transfected and mock control cells at day 8 of culture ($P>0.05$; Figure 2A). By flow-cytometry, 69% c-Kit$^+$/CD71$^+$ cells (equivalent to CFU-E) and 4.2% c-Kit$^+$/CD71$^-$ cells (equivalent to BFU-E) were observed in mock controls at day 8 of culture, whereas 21% c-Kit$^+$/CD71$^+$ cells and 12.6% c-Kit$^+$/CD71$^-$ cells were observed in *Hmgn2*-transfected cells, suggesting that ectopic expression of *Hmgn2* suppressed erythroid differentiation (Figure 2B). Moreover, the percentage of CD71$^+$/Ter119$^+$ cells (equivalent to proerythroblasts) in *Hmgn2*-transfected cells was lower than that seen in mock controls (0.16% versus 1.4%; Figure 2B). Thus ectopic expression of *Hmgn2* inhibited erythroid differentiation of Friend erythroleukaemia cells.

3.3. Hmgn2 misexpression increases the number of erythroleukaemia cells at S-phase of the cell cycle

To investigate how Hmgn2 regulates differentiation of Friend erythroleukaemia cells, the cell cycle status of *Hmgn2*-transfected

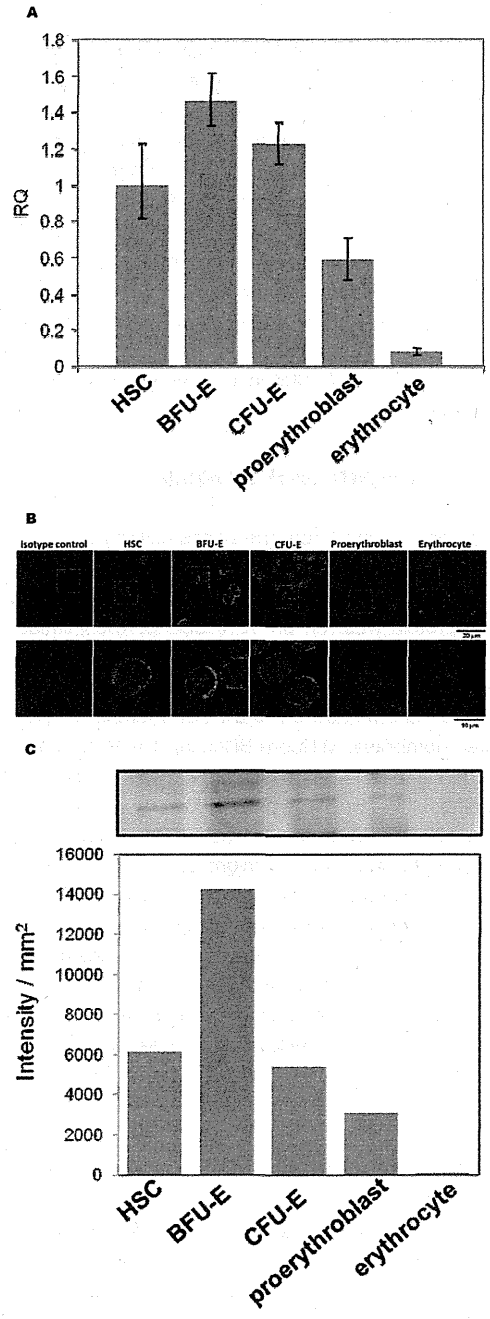

Figure 1 Expression of *Hmgn2* during erythrocyte differentiation in mouse FL
(**A**) Expression of *Hmgn2* in each population of erythroid cells described in Supplementary Figures S1(A) and S1(B) was quantified by RT–PCR. The *y*-axis represents the RQ of gene expression after normalization with β-actin. (**B**) Confocal images of HSCs, BFU-E, CFU-E, proerythroblasts and erythrocytes expressing Hmgn2. Single cells were prepared from mouse FL at 12.5 dpc. Hmgn2 (green) and TOTO®-3 (blue) are shown. Lower panel shows higher magnification of the cells in boxes of upper panel. Scale bars in upper and lower panels indicate 30 and 10 μm respectively. (**C**) WB analysis of Hmgn2 protein in HSCs, BFU-E, CFU-E, proerythroblasts and erythrocytes. Equal amount of protein was trans-blotted on to PVDF membrane and reacted with anti-Hmgn2 antibody. Intensity of protein bands was quantified by Quantity One ver. 4.6.7 and displayed as intensity per mm^2.